Dynamics of a Hole in the Large-U Hubbard Model: A Feynman Diagram Approach

C. Zhou, H. Schulz

J. Phys. I France **5** (1995) 1037–1063 AUGUST **1995**, PAGE 1037

Classification
Physics Abstracts
71.45-d — 72.15Nj — 71.28+d

Dynamics of a Hole in the Large-U Hubbard Model: A Feynman Diagram Approach

C. Zhou and H.J. Schulz

Laboratoire de Physique des Solides(*), Université Paris-Sud, 91405 Orsay, France

(Received 24 January 1995, accepted 2 May 1995)

Abstract. — We study the dynamics of a single hole in an otherwise half-filled two-dimensional Hubbard model by introducing a nonlocal Bogolyubov transformation in the antiferromagnetic state. This allows us to rewrite the Hamiltonian in a form that makes a separation between high-energy processes (involving double-occupancy) and low-energy physics possible. A diagrammatic scheme is developed that allows for a systematic study of the different processes delocalizing a carrier in the antiferromagnetic state. In particular, the so-called Trugman process, important if transverse spin fluctuations are neglected, is studied and is shown to be dominated by the leading vertex corrections. We analyze the dynamics of a single hole both in the Ising limit and with spin fluctuations. The results are compared with previous theories as well as with recent exact small-cluster calculations, and we find good agreement. The formalism establishes a link between weak and strong coupling methodologies.

1. Introduction

Strongly correlated fermion systems have been the focus of interest in the last few years following the discovery of high temperature superconductors. At the heart of the problem is the interplay between the itinerant character of the charge carriers and the existence of localized spins (on some time scale) imposed by the single-occupancy constraint. Considerable effort have been invested in the understanding of the Hubbard model and its strong coupling cousin, the so-called $t-J$ model, in particular in two dimensions. At half filling, the strongly correlated Hubbard model reduces to the Heisenberg model, which is now believed to exhibit antiferromagnetic order on bipartite lattices in two dimensions [1]. Further, for arbitrary correlation strength U, the Hartree-Fock solution leads to a commensurate spin-density wave (SDW) state which approaches the Néel state as U increases [2]. In addition, a straightforward RPA calculation for quantum spin fluctuations has produced a spin wave mode which in the large U limit coincides with what is expected from the Heisenberg model [2,3].

Away from half filling, no consensus exists yet except the Nagaoka theorem. In the weak-correlation limit it is known that doping tends to induce an incommensurate SDW [4]. In

(*) Laboratoire associé au CNRS

particular, the antiferromagnetic state starts to be discommensurated at small doping by deforming into a domain wall structure [4–6]. Increasing the strength of correlations suppresses the amplitude fluctuations, enhancing instead the instability in the transverse channel [6]. In particular, a mean field analysis for the t$-J$ model has predicted a spiral phase [7]. However, inhomogeneous phases have also been argued to be stable at least for small doping even in the large-U limit [8, 9]. So far few substantial studies have been devoted to exploit the effects of quantum fluctuations or to investigate in detail the crossover between weak and strong correlation in the doped case.

Given the different methodologies used in discussing the weakly and strongly correlated regimes of the Hubbard model, it is not at all obvious however why the smooth interpolation should occur. In particular, since weak coupling methods are based on the assumption that the coupling is much less than the bandwidth $8t$, it is unclear how the local constraint of no double occupancy is automatically respected in extrapolating the weak coupling methods to the strong coupling regime. The purpose of the present work is partly to fill that gap. To moderate our ambition we shall limit ourselves only to the case of a single carrier. This will allow us to assume the two-sublattice structure in our analysis, since the antiferromagnetic order is then believed to persist. Moreover, currently available data on finite clusters make reliable quantitative comparisons possible.

The calculations are based on the following idea. By introducing a nonlocal Bogolyubov rotation on the Hubbard Hamiltonian we set up a new basis in which we can readily see the differences and connections between weak and strong coupling approaches. In particular, the low energy scattering processes can be diagrammatically isolated from those at high energy without ambiguity. This in turn makes it possible to show how the latter processes are scaled away as U/t becomes sufficiently large, thus virtually excluding the possibility of double occupancy in the strong coupling limit.

The paper is organized as follows: in Section 2 we introduce the Bogolyubov rotation and derive the effective Hamiltonian within the new basis. In Section 3 we take as example the half-filled case to examine quantum spin fluctuations. The analysis will be performed entirely within the rotated basis in which (1) the Hartree-Fock ground state has exactly the same spin configuration as the unperturbed "noninteracting" state, namely the SDW state; (2) fluctuations above this SDW state can be classified and diagrammatically distinguished according whether double occupancies are involved or not. Such a distinction from the conventional RPA analysis [2, 3, 10] proves to be an important advantage. Based on the observations made in Section 3, the Feynman diagrammatic scheme is then applied to the problem of a single hole in the strongly correlated regime in Section 4. We shall discuss in detail the effects of fluctuations on the dynamics of a single hole and compare with results derived using other available techniques. Comments and a discussion are given in the final Section.

2. The Bogolyubov Transformed Hamiltonian

The standard Hamiltonian of the Hubbard model is

$$H = -t \sum_{\langle i,j\rangle,\sigma} (C^{\dagger}_{i,\sigma} C_{j,\sigma} + h.c.) + U \sum_{i} n_{i,\uparrow} n_{i,\downarrow} \ , \tag{2.1}$$

where the $C_{i,\sigma}$ are annihilation operators for a fermion at site i with spin σ, $n_{i,\sigma}$ is the corresponding number operator, and $\langle i,j\rangle$ indicates summation over the nearest neighbor bonds of a square lattice, each bond being counted once. The ratio between the onsite repulsion parameter U and the hopping energy t determines, together with the bandfilling, the physics of this model. In this section we introduce the Bogolyubov rotation of the fermion operators

and then derive an effective Hamiltonian for the strongly correlated case ($U \gg t$) near half filling.

We begin by going to momentum space and rewriting the Hamiltonian within the reduced Brillouin zone (RBZ) defined by $|k_x| + |k_y| \leq \pi$. This can be done by introducing the spinor notion $\Psi^\dagger_\alpha(\mathbf{k}) = (C^\dagger_{\mathbf{k}\alpha}, C^\dagger_{\mathbf{k}+\mathbf{Q}\alpha})$, where $\mathbf{Q} = (\pm\pi, \pm\pi)$. We then obtain (see Appendix A)

$$\begin{aligned} H &= \sum_{\mathbf{k}\alpha} \varepsilon_{\mathbf{k}} \Psi^\dagger_\alpha(\mathbf{k}) \sigma^3 \Psi_\alpha(\mathbf{k}) \\ &+ \frac{U}{N} \sum_{\mathbf{k}\mathbf{k}'\mathbf{q}} \{\Psi^\dagger_\uparrow(\mathbf{k}+\mathbf{q})\Psi_\uparrow(\mathbf{k})\Psi^\dagger_\downarrow(\mathbf{k}'-\mathbf{q})\Psi_\downarrow(\mathbf{k}') \\ &+ [\Psi^\dagger_\uparrow(\mathbf{k}+\mathbf{q})\sigma^1\Psi_\uparrow(\mathbf{k})][\Psi^\dagger_\downarrow(\mathbf{k}'-\mathbf{q})\sigma^1\Psi_\downarrow(\mathbf{k}')]\} \ , \end{aligned} \tag{2.2}$$

where the σ^i $(i = 1, 2, 3)$ are the standard Pauli matrices, and $\varepsilon_{\mathbf{k}} = -2t(\cos k_x + \cos k_y)$. One should notice that while the summation over momenta runs only over the RBZ, $\mathbf{k} \pm \mathbf{q}$ can freely go beyond the boundaries of the RBZ. Each state is then easily seen to be counted once and only once.

Next we set up a new basis by introducing the following unitary transformation of the fermion operators:

$$\begin{aligned} \Psi_\sigma(\mathbf{k}) &= U_\sigma(\mathbf{k}) R_\sigma(\mathbf{k}) \\ &= \begin{pmatrix} u_{\mathbf{k}} & v_{\mathbf{k}} \\ \sigma v_{\mathbf{k}} & -\sigma u_{\mathbf{k}} \end{pmatrix} \begin{pmatrix} r^c_{\mathbf{k}\sigma} \\ r^v_{\mathbf{k}\sigma} \end{pmatrix} \ , \end{aligned} \tag{2.3}$$

and for $u_{\mathbf{k}}, v_{\mathbf{k}}$ we take the large–U expansion

$$u^2_{\mathbf{k}} = \frac{1}{2}(1 + \frac{2\varepsilon_{\mathbf{k}}}{U}) \qquad , \qquad v^2_{\mathbf{k}} = \frac{1}{2}(1 - \frac{2\varepsilon_{\mathbf{k}}}{U}) \ . \tag{2.4}$$

This, of course, is the Bogolyubov transformation used in the weak coupling approach in diagonalizing the Hartree-Fock Hamiltonian [2,3]. The new operators $r^{c,v}_{\mathbf{k}\sigma}$ are appropriate for particles in an antiferromagnetically-ordered state, and in particular already incorporate the breaking of spin-rotation invariance. Consequently we will see below that the antiferromagnetic ground state is simply obtained by filling the v-states. We emphasize that here the Bogolyubov transformation is applied to the full Hamiltonian instead of the mean-field one, and therefore is exact irrespective of the form of the coefficients $u_{\mathbf{k}}, v_{\mathbf{k}}$. As it will soon be clear this procedure will permit us to examine to what extent the weak coupling approach overlaps with the strong coupling methods.

The transformed Hamiltonian is rather involved when written in momentum space and includes both interband and intraband scatterings as well as conditional single particle interband hoppings. To render things more transparent we turn instead to real space. Assuming $U/t \gg 1$ and keeping only terms up to $O(t^2/U^2)$, we can easily rewrite equation (2.3) in real space and obtain a nonlocal transformation: for the site i on the even sublattice and $\sigma = \downarrow$ or site i on the odd sublattice and $\sigma = \uparrow$ one has

$$C_{i\sigma} = r^v_i - \frac{t}{U} \sum_\delta r^c_{i+\delta} - \frac{J}{8U} \sum_{\delta,\delta'} r^v_{i+\delta-\delta'} \ , \tag{2.5}$$

whereas in the opposite case

$$C_{i\sigma} = r^c_i + \frac{t}{U} \sum_\delta r^v_{i+\delta} - \frac{J}{8U} \sum_{\delta,\delta'} r^c_{i+\delta-\delta'} \tag{2.6}$$

Here $J = 4t^2/U$ as usual, and δ, δ' are nearest–neighbor vectors on the square lattice. The main difference between the new basis and the original one is thus very clear: the electrons are now classified in terms of the category (c or v) they belong to, instead of spin: a v electron has spin $\downarrow$ if it sits on the even sublattice and spin $\uparrow$ if it sits on the odd sublattice, and *vice versa* for the c–electrons. Thus, a fully occupied v–band is essentially a Néel ordering in the original basis (namely, we observe a down spin on the even sublattice and an up spin on the odd sublattice). We note that the particles created by the r–operators are not strictly localized on their respective sites, but are rather in the Wannier states corresponding to the mean–field Néel state and thus are to a certain degree delocalized on nearest (amplitude $\propto t/U$) and next–nearest (amplitude $\propto (t/U)^2$) neighbors.

The effective Hamiltonian is finally obtained by substituting the above transformation into the Hubbard Hamiltonian. We thus have, retaining only terms up to $O(t^2/U)$:

$$H = H_1 + H_2 + H_d \ , \tag{2.7}$$

$$\begin{aligned} H_1 = & - t \sum_{i\delta} \{(1 - n_i^v) r_i^{c\dagger} r_{i+\delta}^v (1 - n_{i+\delta}^c) + \text{h.c.}\} \\ & + 2J \sum_i (n_i^c - n_i^v) - J \sum_{\langle i,j \rangle} (S_i^z S_j^z - \frac{1}{4} n_i n_j) + \frac{J}{2} \sum_{\langle i,j \rangle} (S_i^+ S_j^- + S_i^- S_j^+) \ , \end{aligned} \tag{2.8}$$

$$\begin{aligned} H_2 = & \frac{J}{2} \sum_{i,\delta \neq \delta'} (r_i^{c\dagger} r_{i+\delta-\delta'}^c - r_i^{v\dagger} r_{i+\delta-\delta'}^v) + \frac{J}{4} \sum_{i,\delta \neq \delta'} (n_i^c r_{i+\delta}^{c\dagger} r_{i+\delta\prime}^c + n_i^v r_{i+\delta}^{v\dagger} r_{i+\delta\prime}^v) \\ & - \frac{J}{4} \sum_{i,\delta \neq \delta'} (r_i^{c\dagger} r_{i+\delta}^v r_{i+\delta'}^{c\dagger} r_i^v + \text{h.c.}) \ , \end{aligned} \tag{2.9}$$

$$\begin{aligned} H_{\text{d}} = & U \sum_i n_i^c n_i^v + t \sum_{i\delta} (n_i^c r_i^{v\dagger} r_{i+\delta}^c n_{i+\delta}^v + h.c.) \\ & - \frac{J}{4} \sum_{i,\delta\delta'} (r_i^{c\dagger} r_{i+\delta}^v r_i^{v\dagger} r_{i+\delta'}^c + \text{h.c.}) - \frac{J}{8} \sum_{i,\delta\delta'} \{n_i^c (r_i^{v\dagger} r_{i+\delta-\delta'}^v + h.c.) + c \leftrightarrow v\}. \end{aligned} \tag{2.10}$$

The spin index in the original Hamiltonian now is replaced by the v and c band indices, as discussed following equations (2.5) and (2.6). The spin operators in H_1 are defined by $S_i^+ = r_i^{c\dagger} r_i^v$ on the even sublattice and $S_i^- = r_i^{c\dagger} r_i^v$ on the odd sublattice and represent local spin flips in the *new* basis. Further, $n_i n_j/4 - S_i^z S_j^z$ in H_1 is a rewriting of $(n_i^c n_j^c + n_i^v n_j^v)/2$ which represents nearest neighbor intraband scattering. We have expressed the Hamiltonian in three terms, namely H_1, H_2, H_d, to emphasize the fact that all interaction processes in H_{d} involve double occupancy, and in H_2 the electrons will always go beyond the nearest neighbors. We also notice that in H_1 and H_{d} there are terms involving six fermionic operators. These terms in fact cancel (not surprisingly, given that the original Hamiltonian only involves terms containing up to four fermion operators and that the transformation to the new operators is linear), however, we find the forms (2.8), (2.10) rather useful because they clearly separate terms involving double occupancy from those which do not. We note that an alternative way to derive the from of the Hamiltonian given by equations (2.7) to (2.10) is to first diagonalize the antiferromagnetic Hartree–Fock Hamiltonian and then to express the terms omitted by the new quasiparticle operators, taking the large–U limit.

It is worthwhile here discussing the different terms appearing in the "double-occupancy" Hamiltonian $H_{\rm d}$. The first term clearly just counts the number of doubly occupied sites and gives a (large) energy U for each doubly occupied site. The second (order t) term, because of the $n^{c,v}$ operators involved, only moves a particle from a doubly occupied site to an already occupied site, i.e., the number of doubly occupied sites is conserved by this term. The first two terms thus act entirely within a (high-energy) subspace of a given number of doubly occupied sites. The third term creates two particles on a previously unoccupied site or destroys two particles on a doubly occupied site, and the fourth term creates a particle on a previously occupied site or destroys a particle on a previously doubly occupied site, Thus, these two terms, both of order J, couple the subspace without double occupancy to the subspace with double occupancy. In the following we will be interested in states with at most one fermion per site. The corrections one obtains from $H_{\rm d}$ then are negligible as far as low energy properties are concerned: the coupling terms between the at most singly occupied subspace and the subspace involving double occupancy are of order J, whereas the intermediate state created has an energy of order U, i.e., one expects corrections of order $J^2/U = 16t^4/U^3$. This is clearly a higher order correction compared to the terms of order J which we have retained in H_1 and H_2.

It is clear that at half-filling (one electron per site) the "non-interacting" (or Hartree-Fock) ground state of the transformed Hamiltonian (2.7) is not the paramagnetic Fermi sea as in the original basis, but rather a state with all the v-states filled and all the c-states are empty. That is to say that in the new basis electrons will first fill the v-band in which the spin of each electron is seen to point down on the even sublattice and up on the odd sublattice. The symmetry breaking is of course due the form of the Bogolyubov transformation that is already adapted to the antiferromagnetic order of the ground state. The Hartree-Fock energy of the ground state state is $E_0 = -NJ$.

The Hartree-Fock quasiparticle energies are obtained by calculating the average value of H in a state with either a c-particle added or a v–particle taken out. We define k-space operators by

$$r_{\mathbf{k}}^{c,v} = \frac{1}{\sqrt{N}} \sum_i r_i^{c,v} e^{i\mathbf{k}\cdot\mathbf{R}_i} \quad , \tag{2.11}$$

with the k-summation covering the full Brillouin zone, and obtain

$$H_{\rm HF} = \sum_{\mathbf{k}} (\xi_{\mathbf{k}}^c r_{\mathbf{k}}^{c\dagger} r_{\mathbf{k}}^c + \xi_{\mathbf{k}}^v r_{\mathbf{k}}^{v\dagger} r_{\mathbf{k}}^v) - NJ \quad , \tag{2.12}$$

where the quasiparticle energies are $\xi_{\mathbf{k}}^c = U - J + \varepsilon_{\mathbf{k}}^2/U$ and $\xi_{\mathbf{k}}^v = J - \varepsilon_{\mathbf{k}}^2/U$. These expressions of course agree with the large–U limit of previous Hartree-Fock calculations [2, 3]. We note that the operators thus defined are *not* eigenfunctions of σ_z, because the spin projection of, e.g., a v-particle is different on the even and odd sublattice. Spin eigenstates can however be straightforwardly constructed noting that $\xi_{\mathbf{k}}^{c,v} = \xi_{\mathbf{k}+\mathbf{Q}}^{c,v}$. The operators with well-defined spin then are $r_{\mathbf{k}\sigma}^{c,v} = (r_{\mathbf{k}}^{c,v} \pm r_{\mathbf{k}+\mathbf{Q}}^{c,v})/\sqrt{2}$, where k-space is now limited to the *reduced* Brillouin zone. In terms of these operators the Hartree-Fock Hamiltonian takes the form

$$H_{\rm HF} = \sum_{\mathbf{k}\sigma} (\xi_{\mathbf{k}}^c r_{\mathbf{k}\sigma}^{c\dagger} r_{\mathbf{k}\sigma}^c + \xi_{\mathbf{k}}^v r_{\mathbf{k}\sigma}^{v\dagger} r_{\mathbf{k}\sigma}^v) - NJ \quad . \tag{2.13}$$

The c-band is now seen to be separated from the fully occupied v-band by a gap of order U. In addition, the Hartree-Fock ground state at half-filling has a fully filled v-band and an empty c-band corresponding to Néel spin ordering.

Going back to the full Hamiltonian (2.7) it is clear that for electron density $n \leq 1$ the c-band is drawn in only through *interband* interactions. To get an idea how the c-band becomes involved, we notice that interband interactions can actually be divided into two classes. Interband processes described in H_d can bring in the c-band but always provoke double occupancy simultaneously. At the Hartree-Fock level this of course pushes the c-band by U above the v-band, and it is clear that beyond Hartree-Fock, there will always an intermediate state of energy $\approx U$ involved. We have already seen that the virtual interband transitions in H_d can only give rise to a correction of order J^2/U. On the other hand, interband processes contained in $H_1 + H_2$ can actually transfer the v-band electrons to the c-band or *vice versa* at much less energy expense. One such example is the interchange of two nearest neighboring v-band particles. This amounts to having a spin flip at each site since these two particles have opposite spins, or equivalently the pair of v-band particles hops to the c-band in the end. Such a process is realized via the interband pair hoping described by the last term in H_1 and costs only an energy of order $O(J)$.

It is physically clear that scatterings involving double occupancy will actually be circumvented in the strong coupling limit and therefore render no substantial contribution to the low energy physics. Nevertheless, this is not so obvious if we deal directly with the Hubbard model using Feynman's diagrammatic technique. It turns out and will be shown below that the advantage of the Bogolyubov rotation proposed here is that it provides a basis in which we are able to clearly demonstrate with Feynman diagrams the irrelevance of H_d in the effective low energy properties.

Once established that H_d will eventually be scaled away, we are left with $H_1 + H_2$ to describe low energy physics of the large-U Hubbard model. In particular, H_1 is scarcely different from the familiar $t - J$ model, except for the interactions in the (charge and spin) density channel. Here we note that the "noninteracting" state we start with in the new basis exhibits Néel ordering. The spin fluctuations above the Néel state are then of ferromagnetic nature in the longitudinal spin channel. On the other hand, since the spin rotational symmetry has been retained in the transformation fluctuations in the transverse spin channel are described in exactly the same manner as in the $t - J$ model.

3. Quantum Fluctuations at Half Filling

We devote this section to the discussion of quantum spin fluctuations in the half-filled Hubbard model. The final result is actually known either from spin wave calculations or from direct extrapolation of weak-coupling results. The convergence of these apparently unrelated approaches raises the question of a possible smooth crossover between the two extreme coupling regimes. The main point which remains unclear is why and how the local constraint of no double occupancy becomes automatically respected when one goes to large U within the mean-field formalism which is frequently believed to be limited to weak coupling. The purpose of our presentation is to demonstrate that within the new basis we are able to show explicitly and in Feynman diagrams how the higher energy processes involving double occupancies (i.e., H_d) are in the end scaled away and become irrelevant to the spin dynamics.

The antiferromagnetic ordering implies the the existence of gapless spin wave excitations in the transverse spin channel. This can be analyzed by studying the dynamical spin susceptibility in the presence of Néel ordering which is now defined as a 2×2 matrix:

$$\chi^{-+}(\mathbf{x}, \mathbf{x}', t) = -i \begin{pmatrix} \langle T\left(\bar{S}^-_{x_e}(t)\bar{S}^+_{x'_e}(0)\right)\rangle & \langle T\left(\bar{S}^-_{x_e}(t)\bar{S}^+_{x'_o}(0)\right)\rangle \\ \langle T\left(\bar{S}^-_{x_o}(t)\bar{S}^+_{x'_e}(0)\right)\rangle & \langle T\left(\bar{S}^-_{x_o}(t)\bar{S}^+_{x'_o}(0)\right)\rangle \end{pmatrix} \tag{3.1}$$

As convention, the position coordinate $\mathbf{x}$ is denoted by $\mathbf{x_e}$ if the spin is on the even sublattice and by $\mathbf{x_o}$ if on the odd sublattice. We have added a bar over the spin operators in order to emphasize that we are probing correlations between spins defined in terms of the original C–operators (as opposed to the S–operators occurring in equation (2.8)).

The calculation for the above matrix at the Hartree-Fock level is straightforward. We first transform the susceptibility matrix such that $\bar{S}^+$, $\bar{S}^-$ are written in terms of r-operators as presented in Appendix B. The leading contribution is then readily obtained. Up to $O(J/U)$ only the diagonal terms in equation (3.1) are nonzero and are given by

$$\chi^{-+}_{\mathrm{HF}11}(\mathbf{q},\omega) = \chi^{-+}_{\mathrm{HF}22}(\mathbf{q},-\omega) = \frac{2}{N}\sum_{\mathbf{k}} \frac{1}{\omega - \xi^c_{\mathbf{k}-\mathbf{q}} + \xi^v_{\mathbf{k}} + i0^+} \quad . \tag{3.2}$$

With little algebra [11] one can verify that this agrees with the results [2] of SWZ up to $O(J/U)$.

To calculate the dynamical susceptibility in the presence of interactions we need to take some care. In all previous studies [2,3,10], the RPA scheme was adopted within the *paramagnetic* C-operator basis in which the interaction in the transverse spin channel is exactly U. Here we rather write the original spin operators ($\bar{S}$) in terms of the r-operators. Then the simplest Hartree-Fock ground state already has the correct antiferromagnetic structure, and the interaction between the Hartree-Fock particles is directly obtained from equations (2.7)–(2.10). To facilitate the following discussion we write the interaction explicitly in momentum space. The terms relevant for the transverse spin fluctuations (3.1) are

$$\begin{aligned} H_I^{+-} \;=\; & \frac{2}{N}\sum_{\mathbf{k}\mathbf{k}'\mathbf{q}} \Big(g_1(\mathbf{k},\mathbf{k}') r^{c\dagger}_{\mathbf{k}+\mathbf{q}\downarrow} r^{v\dagger}_{\mathbf{k}'-\mathbf{q}\uparrow} r^{v}_{\mathbf{k}\uparrow} r^{c}_{\mathbf{k}'\downarrow} + g_2(\mathbf{k},\mathbf{k}') r^{c\dagger}_{\mathbf{k}\downarrow} r^{c\dagger}_{\mathbf{k}'-\mathbf{q}\uparrow} r^{v}_{\mathbf{k}-\mathbf{q}\uparrow} r^{v}_{\mathbf{k}'\downarrow} \\ & + v \longleftrightarrow c \Big) \quad , \end{aligned} \tag{3.3}$$

with

$$g_1(\mathbf{k},\mathbf{k}') = U\left[1 - \frac{\varepsilon^2_{\mathbf{k}} + \varepsilon^2_{\mathbf{k}+\mathbf{q}} + \varepsilon^2_{\mathbf{k}'} + \varepsilon^2_{\mathbf{k}'-\mathbf{q}}}{2U^2}\right] \quad , \tag{3.4}$$

$$g_2(\mathbf{k},\mathbf{k}') = -\frac{\varepsilon_{\mathbf{k}}\varepsilon_{\mathbf{k}-\mathbf{q}} + \varepsilon_{\mathbf{k}'}\varepsilon_{\mathbf{k}'-\mathbf{q}}}{U} \tag{3.5}$$

We note that no $O(t)$ terms enter as can easily be understood for half filling. Neither do the intraband interactions enter since they contribute only to longitudinal fluctuations. H_I^{+-} is now composed of two parts. The g_1 part is equivalent to the first two terms in H_d and describes interband scatterings involving double occupancy. On the other hand, the g_2 part describes the transfer of a pair of particles between two bands and corresponds to the last terms in H_1 and H_2. This part will be shown to be the one responsible for the spin dynamics. Finally it will be helpful to note that up to $O(J/U)$, g_1 and g_2 can actually be factorized by $g_1 = U f_1(\mathbf{k}) f_1(\mathbf{k}')/4$ and $g_2 = U(f_1(\mathbf{k}) f_2(\mathbf{k}') + f_1(\mathbf{k}') f_2(\mathbf{k}))/4$, with f_1 and f_2 being defined in Appendix B.

We are now in the position to study the transverse spin fluctuations in the SDW state. Following Appendix B we shall calculate

$$\chi^{-+}(\mathbf{q},\omega) = -\frac{i}{2N}\sum_{\mathbf{k}\mathbf{k}'} f_1(\mathbf{k}) f_1(\mathbf{k}') \begin{pmatrix} a_{11} & a_{12} \\ a_{21} & a_{22} \end{pmatrix} \tag{3.6}$$

to get the dominant contribution. The definition for the matrix elements is given in Appendix B. A slight complication arises in the calculation due to the fact that in the interaction Hamiltonian H^{+-} two interaction vertices g_1 and g_2 are involved, and both of them are momentum-dependent. However, we should notice that the g_1 interaction conserves the number of particles

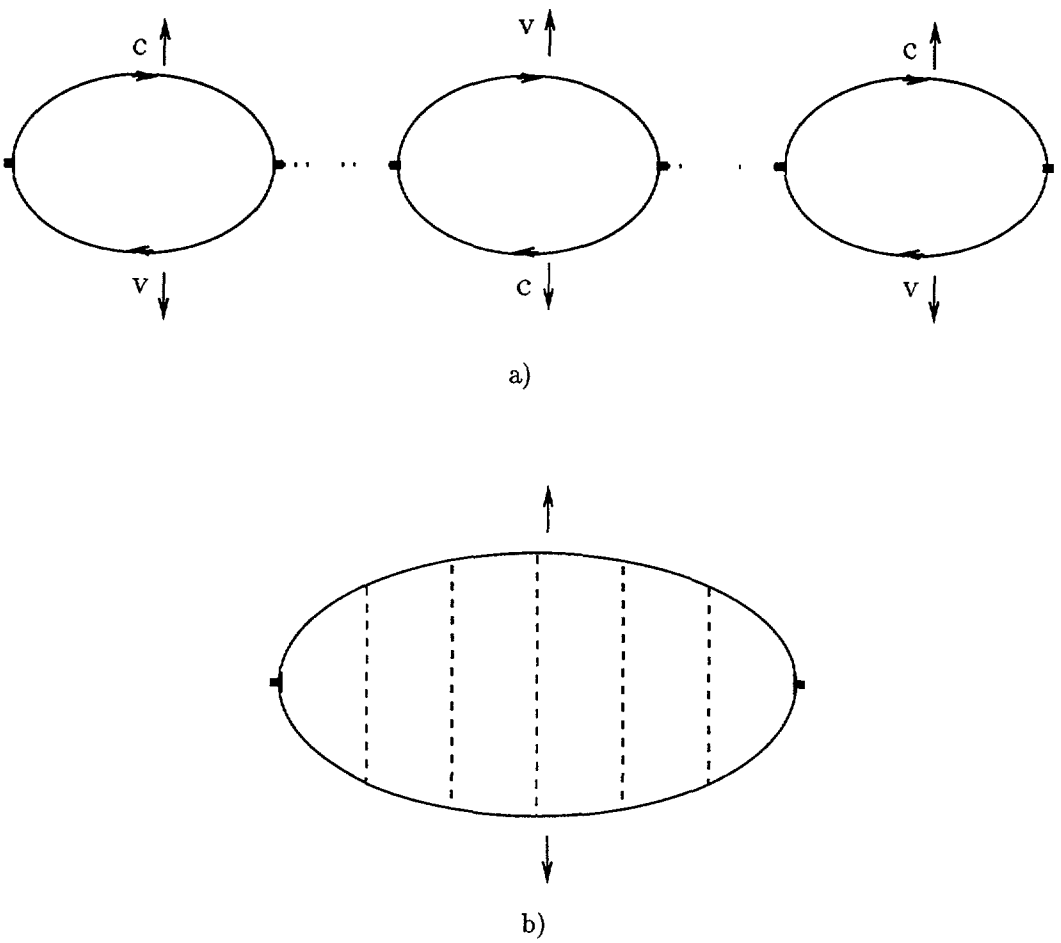

Fig. 1. — a) The RPA scheme for the spin-spin correlation function (χ_{11}) in the transverse spin channel. The dotted lines between bubbles denote the g_2 interactions. The "bare" bubble here is the result of (b); b) The interband multiple scatterings between a c-particle and v-hole, which result in the renormalized "bare" bubble used in (a). The interaction vertex in the ladder are g_1.

in each band. In other words, for an excited particle-hole pair of opposite spin the g_1-term contributes to multiple scatterings between the particle and hole. On the contrary g_2-interactions give rise to destruction and formation of p–h pairs of different spins. Within the RPA scheme we then find that g_1 and g_2 will operate distinctly and the two interactions do not mix up in Feynman diagrams. A typical diagram for χ^{-+} incorporating both interactions is shown in Figure 1.

Having learnt that the g_1- and g_2-type interactions do not mix up at RPA level, we can deal with them separately. Let us look at the g_1-interaction first. As is evident, the off-diagonal terms in equation (3.6) remains zero with only g_1 interactions. To get the diagonal terms of equation (3.6), we need to evaluate the diagram illustrated in Figure 1b. After a

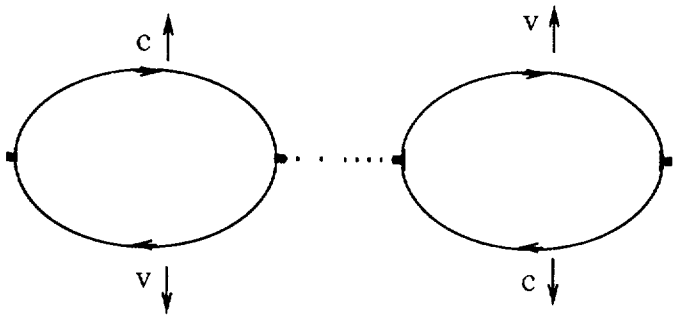

Fig. 2. — The first-order nonzero contribution to χ_{21} in equation (3.6). The "bare" bubble in the figure is the g_1-renormalized result given in Figure 1b. As in Figure 1 the dotted lines denotes the g_2 interactions.

straightforward calculation we obtain

$$\chi^{-+}_{11(22)}(\mathbf{q},\omega) = \frac{\frac{1}{2N}\sum_{\mathbf{k}} f_1^2(\mathbf{k})A(\mathbf{k},\mathbf{q})}{1+\frac{U}{2N}\sum_{\mathbf{k}} f_1^2(\mathbf{k})A(\mathbf{k},\mathbf{q})} \quad , \tag{3.7}$$

where $1/A(\mathbf{k},\mathbf{q}) = \pm\omega - \xi^c_{\mathbf{k}-\mathbf{q}} + \xi^v_{\mathbf{k}} + i0^+$. In particular, taking the limit of $U \gg t$ gives the g_1-renormalized susceptibility as

$$\chi_0^{-+}(\mathbf{q},\omega) = \begin{pmatrix} \chi^0(\mathbf{q},\omega) & 0 \\ 0 & \chi^0(\mathbf{q},-\omega) \end{pmatrix} \quad , \tag{3.8}$$

$$\chi^0(\mathbf{q},\omega) = \frac{1}{\omega - 2J + i0^+} \tag{3.9}$$

We notice that going from equation (3.2) to equations (3.8) and (3.9) the high energy scale of $O(U)$ has disappeared due to the renormalization by multiple g_1 scatterings and has been replaced by $2J$ which is the energy one needs to create a local spin flip. This is natural because after all a local spin flip can occur without involving double occupancies.

Finally we switch on the g_2 interactions. As explained before and shown in Figure 1 within RPA they have no effect on the structure within the bubble but play their role by forming junctions between g_1-renormalized bubbles. Besides, g_2 interactions also render a nonzero contribution to off-diagonal terms a_{12} and a_{21} in equation (3.6), as is shown diagrammatically in Figure 2. Again the work involved in the calculation is routine since g_2 also factorizes as $g_2(\mathbf{k},\mathbf{k}') \sim (f_1(\mathbf{k})f_2(\mathbf{k}') + f_1(\mathbf{k}')f_2(\mathbf{k}))$. We only mention that because of the way in which g_2 is factorized, we shall meet in the intermediate states bubble diagrams like Figure 1b but with vertex parts f_1 or f_2 attached to one of its two legs. For example, when f_1 is attached to one leg and f_2 to the other, the diagram gives $4J\gamma_{\mathbf{q}}/(U(\pm\omega - 2J))$, whereas f_2 is attached to both legs leads to $4J^2\gamma^2_{\mathbf{q}}/(U^2(\pm\omega - 2J))$. The final result for the susceptibility then is obtained as

$$\chi^{-+}(\mathbf{q},\omega) = -\frac{2J}{\omega^2_{\mathbf{q}} - \omega^2} \begin{pmatrix} 1+\frac{\omega}{2J} & -r_{\mathbf{q}} \\ -r_{\mathbf{q}} & 1-\frac{\omega}{2J} \end{pmatrix} \quad , \tag{3.10}$$

where $\omega_{\mathbf{q}} = 2J\sqrt{1-r^2_{\mathbf{q}}}$ is the standard spin wave spectrum. The same expressions can be found from Singh and Tesanovic's results [3, 12] by directly extrapolating the RPA results. However, with the help of Bogolyubov rotation and by working within the rotated basis we

have explicitly shown here how the higher energy scale gets irrelevant in the spin dynamics within the framework of a diagrammatic approach.

At last, we point out that the above results can equally be derived by considering only H_1 and neglecting H_2 and H_d entirely, using the same Feynman diagrammatical scheme. From the Hartree-Fock solution of H_1 we immediately get equation (3.8), and the final result of equation (3.10) is obtained following RPA for the Heisenberg exchange interactions in the transverse spin channel. The coincidence teaches us two things. First, it shows that the $t-J$ model represents the Hubbard model more faithfully in the strongly correlated regime than the $t-J-J'$ or $t-t'-J$ models. Secondly, one sees that it is possible to extend the Feynman diagrammatic technique to the strong coupling regime by working directly within the sub–Hilbert space of no double occupancy. In the next two sections we shall use this fact to discuss the dynamics of a single hole in the otherwise quantum antiferromagnetic background.

4. The Dynamics of a Single Hole

We now begin to examine the motion of a hole in the antiferromagnetic environment. For this purpose we take away one down spin electron from the v–band and study the Green's function for the v–band hole thus created

$$\mathcal{G}^v_\sigma(\mathbf{k},t) = -i\langle 0|T(r^{v\dagger}_{\mathbf{k}\sigma}(t)r^v_{\mathbf{k}\sigma})|0\rangle \tag{4.1}$$

within the sub-Hilbert space of no double occupancy, as defined in the last section. Here $|0\rangle$ represents the full v-band, i.e., the Néel state. The Fourier transform of (4.1) generally contains two terms, corresponding to particle and hole propagation, respectively. However in the present case of a single hole only the hole term actually remains:

$$\mathcal{G}^v_\sigma(\mathbf{k},\omega) = \langle 0|r^{v\dagger}_{\mathbf{k}\sigma}\frac{1}{\omega - H + i0^+}r^v_{\mathbf{k}\sigma}|0\rangle \tag{4.2}$$

The $+i0^+$ in equation (4.2) emphasizes that we are considering hole propagation in the following. For the reason given at the end of the last section, and also to render possible a direct comparison with available numerical results obtained notably for the $t-J(J_z)$ model we shall in the following (and unless specified otherwise) neglect H_2 which always leads to jumps beyond the nearest neighbors. The principal subject we shall deal with is therefore H_1.

To begin we shall also neglect (transverse) spin fluctuations altogether ($t-J_z$ model). The Hartree-Fock state of H_1 is defined by two degenerate energy levels ($\omega_v = 0$ and $\omega_c = 2J$ respectively), and the bare c and v particles are completely immobile, i e., their propagator is non-zero only if creation and destruction operators act on the same site. We also for the moment neglect interactions in the longitudinal channel (the third term in H_1). The effect of this interaction will be included below (see Eq. (4.15) and the corresponding discussion). The only remaining interaction in H_1 then is the $O(t)$ hopping term which takes effect when a hole is introduced and is allowed to move:

$$H_I = -t\sum_{i\delta}\{(1-n^v_i)r^{c\dagger}_i r^v_{i+\delta}(1-n^c_{i+\delta}) + (1-n^c_{i+\delta})r^{v\dagger}_{i+\delta}r^c_i(1-n^v_i)\} \ . \tag{4.3}$$

Obviously, this term correlates the hopping motion of a particle (or hole) with the occupation of its surrounding sites and thus is responsible for the coupling between the moving hole and its Néel environment. In principle, this form can be used for a diagrammatic study of the Green's function. However, in the following it will be enough to consider the simpler form

$$H_I = -t\sum_{i\delta}\{(1-n^v_i)r^{c\dagger}_i r^v_{i+\delta} + r^{v\dagger}_{i+\delta}r^c_i(1-n^v_i)\} \ , \tag{4.4}$$

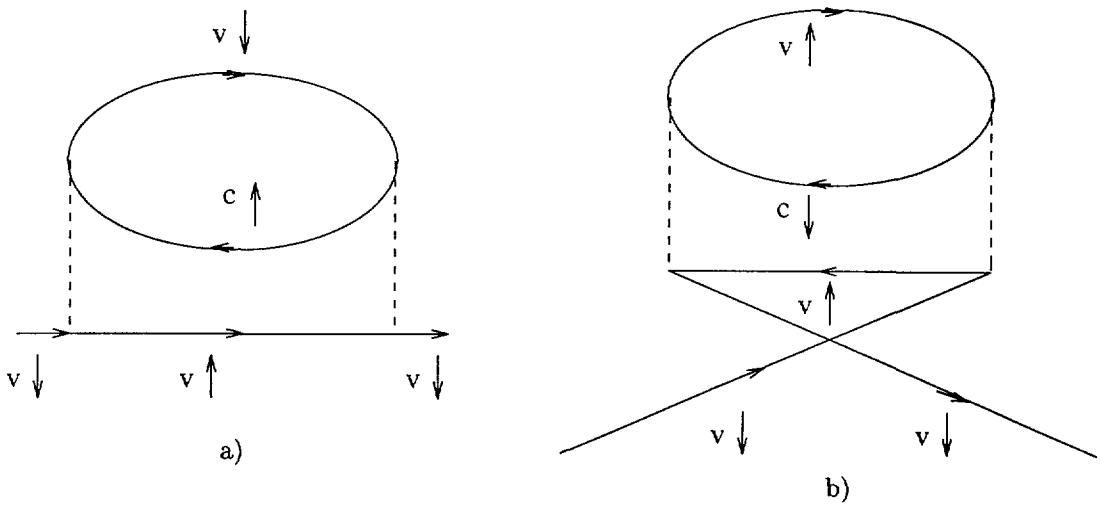

Fig. 3. — The second-order correction to the hole selfenergy. For a down spin hole, (a) is determined by the first term in H_I, while (b) by the second term. (b) does not contribute in the absence of spin fluctuations (see text). The dashed line joining the bubble and the hole line denotes the $O(t)$ interactions in H_I. The continuous line represents a v-hole jumping to a nearest-neighbor site (and therefore flipping spin), and the c, v particle-hole pair is created on the same site.

which now contains four-fermion terms only. Acting on states containing only empty and singly occupied sites as in (4.2) the first terms in (4.3) and (4.4) are easily seen to be identical. On the other hand, the second term in (4.4) can create double occupancy, which is prohibited by the factor $(1 - n^c_{i+\delta})$ in (4.3). In the subsequent diagrammatic development we therefore will have to take care to avoid processes creating double occupancy. It will turn out that this is actually rather straightforward in the present scheme.

For later convenience we write down its Fourier transform in the RBZ explicitly:

$$H_I = -\frac{2}{N}\sum_{\mathbf{k}\mathbf{k}'\mathbf{q}} \{\varepsilon_{\mathbf{k}} \tilde{r}^{v\dagger}_{\mathbf{k}'\uparrow} \tilde{r}^{v}_{\mathbf{k}'+\mathbf{q}\uparrow} \tilde{r}^{v\dagger}_{\mathbf{k}\downarrow} \tilde{r}^{c}_{\mathbf{k}-\mathbf{q}\downarrow} + \varepsilon_{\mathbf{k}'} \tilde{r}^{v\dagger}_{\mathbf{k}\downarrow} \tilde{r}^{v}_{\mathbf{k}-\mathbf{q}\downarrow} \tilde{r}^{c\dagger}_{\mathbf{k}'-\mathbf{q}\uparrow} \tilde{r}^{v}_{\mathbf{k}'\uparrow} + \text{h.c.}\} \ , \tag{4.5}$$

where $\varepsilon_{\mathbf{k}} = -zt\gamma_{\mathbf{k}} = -2t(\cos(\mathbf{k}_x) + \cos(\mathbf{k}_y))$ and z is the coordination number. We note in particular that the momentum in $\varepsilon_{\mathbf{k}}$ is always that of the the v–band hole which has the same spin as the c–particle. This fact will be used on numerous occasions when we need to determine vertex functions. In addition, the hole notation $\tilde{r} = r^\dagger$ has been introduced in order to facilitate the discussion.

4.1. THE INCOHERENT SPECTRUM. — It is evident that the first nonzero contribution arises only in the second order correction to the selfenergy. Naively one would have expected, as is readily derived from the interaction Hamiltonian, contributions from the two diagrams shown in Figure 3. Nevertheless, in the absence of spin fluctuations the contribution from Figure 3b vanishes since the lower $(v, \uparrow)$ line represents hole propagation, which implies that the $(c, \downarrow)$ line should represent creation of a hole in the c band. This of course is impossible, the c band being initially empty. In other words, a pair of a *c–particle* and a *v–hole* of opposite spins can not appear *before* the hole starts moving. Consequently for an initial down spin hole we only see in the intermediate state an up spin hole, accompanied by a p–h pair formed by c–band

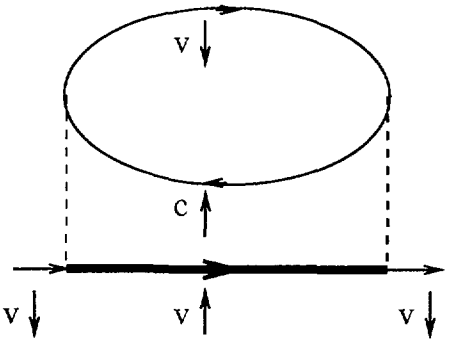

Fig. 4. — The selfconsistent second-order correction to the self-energy which accounts for the incoherent background in the hole spectrum.

up spin particle and v–band down spin hole. The diagram is then evaluated according to the standard Feynman rules and is given by:

$$\Sigma^v_\downarrow(\mathbf{k},\omega+i0^+) = i\frac{2z^2t^2}{N}\sum_{\mathbf{k}_1}\gamma^2_{\mathbf{k}_1}\int\frac{\mathrm{d}\omega_1}{2\pi}\mathcal{G}^{v(0)}_\uparrow(\mathbf{k}_1,\omega_1+i0^+)\chi^0(\mathbf{k}-\mathbf{k}_1,\omega-\omega_1)\ . \tag{4.6}$$

The hole notation has been emphasized in the expression by $\omega + i0^+$ such that the Green function of a hole below the Fermi sea is seen as a retarded function of time. The noninteracting Green function is therefore $\mathcal{G}^{v(0)} = 1/(\omega + i0^+)$, the p–h bubble is easily determined and is given by equation (3.9), which is also a retarded function. Moreover, the vertex functions at two interacting lines are all determined by the momentum $\mathbf{k}_1$ of the scattered hole in the intermediate state. We thus obtain as final result:

$$\Sigma^v_\downarrow(\mathbf{k},\omega) = \frac{zt^2}{\omega-2J}\ . \tag{4.7}$$

The factor z reflects the fact that the hole moves to its z nearest neighbors. The absence of momentum dependence corresponds to the fact that the approximation actually binds holes to its origin by allowing only back and forth motions towards its nearest neighbors (as implied by the momentum summation over $\gamma^2_{\mathbf{k}}$). The particle-hole pair in Figure 3a is easily seen to represent the local spin flip the hole leaves behind at its initial position once it hops.

A more complete picture arises when we introduce selfconsistency in Figure 3a. The procedure is immediately seen to permit the intermediate up spin hole to move further forward. The new Feynman diagram (Fig. 4) requires us to solve the following selfconsistency equation:

$$\Sigma^v_\sigma(\mathbf{k},\omega+i0^+) = i\frac{2z^2t^2}{N}\sum_{\mathbf{k}_1}\gamma^2_{\mathbf{k}_1}\int\frac{\mathrm{d}\omega_1}{2\pi}\mathcal{G}^v_{-\sigma}(\mathbf{k}_1,\omega_1+i0^+)\chi^0(\mathbf{k}-\mathbf{k}_1,\omega-\omega_1) \tag{4.8}$$

After substituting the bare particle-hole bubble, equation (3.9), the coupled equations for Σ and $\mathcal{G}$ are further reduced to a simple iterative equation for the spin and momentum independent Green function:

$$\mathcal{G}^v(\omega) = \frac{1}{\omega - zt^2\mathcal{G}^v(\omega-2J)} \tag{4.9}$$

This agrees with the result of Shraiman and Siggia for the incoherent hole spectrum [13, 14].

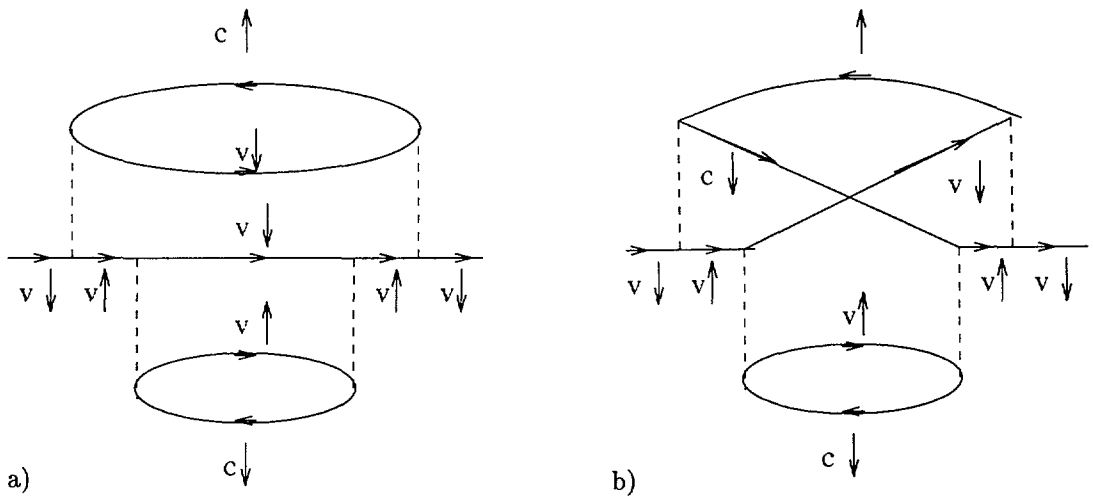

Fig. 5. — A typical selfenergy diagram in the Shraiman-Siggia limit a), and b) a diagram neglected in the selfconsistent scheme. Diagrams of type b) need to be included in order to avoid overcounting of self-crossing paths.

The physics is rather clearly reflected in the diagrammatic picture. Because of the selfconsistency, the selfenergy is now described by a series of Feynman diagrams of order $2, 4, 6, \ldots$ At a typical order $2n$ (Fig. 5), a sequence of n bubbles is first formed and the bubbles are then eliminated one after another in *reversed* order. Since a momentum-independent bubble of opposite spins in the Feynman diagrams means a local spin flip in real space, the above sequence describes actually a string of overturned spins in the intermediate state. In addition, the number of bubbles n is the length of the string for that particular order. In conclusion the selfconsistency has, on the one hand, made possible to allow for infinitely many particle-hole excitations in the intermediate states along the way the hole hops forward; on the other hand it guarantees that the hole can only follow the self-retracable paths defined by Brinkman and Rice [15] and remains bound to its original position. We have thus incorporated the contributions from incoherent excitations within the diagrammatic scheme. We notice that the diagrams we consider here do not create double-occupancy: the second term in equation (4.4) only creates double occupancy if the c-particle annihilates with a v-hole different from the one it was initially created with. Such diagrams do not appear here, nor in the processes considered below.

The numerical solution of equation (4.9) defines a ladder spectrum or a sequence of bound states, with the lowest state being order of $t(J/t)^{2/3}$ above the lower edge of the Brinkman-Rice band $\omega_0 = -2\sqrt{z}t$. The discrepancy with the original $-2\sqrt{z-1}t$ of Brinkman and Rice [15] is understood according to Kane *et al.* [16]: in summing $\gamma_{\mathbf{k}}^2$ in equation (4.8) contributions from all the nearest neighbors are assumed at every stage of the intermediate states. This results in overcounting from the second step on, since in fact only forward going steps should be counted [14], giving rise to self-avoiding paths. To correct the overcounting within the diagrammatic scheme, it would be necessary to insure that the overturned spin created by the movement of the hole is not situated on an already overturned site, e.g., the Pauli principle has to be taken into account in the intermediate states. This in principle can be achieved by adding diagrams involving v-v exchange. The appropriate diagram at fourth order in t is shown in Figure 5, and one easily can construct the corresponding higher-order diagrams. We

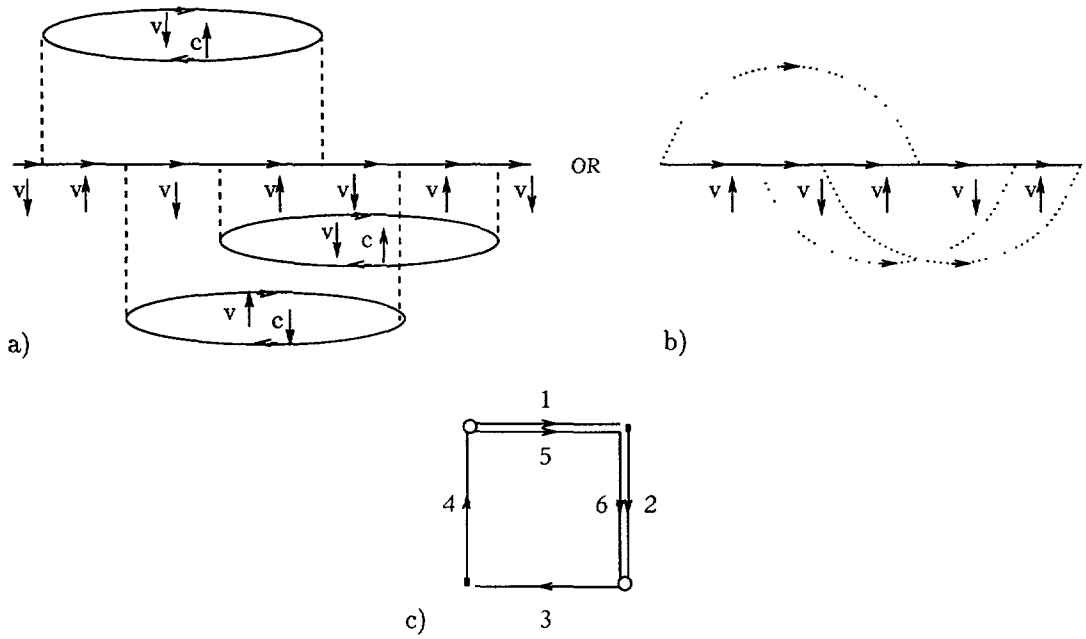

Fig. 6. — The leading vertex correction in the Ising limit. b) is an equivalent of a), in which the particle-hole bubble is denoted by a dotted line; c) The real space configuration corresponding to a) or b).

will not attempt here to sum these diagrams, but rather introduce the ad hoc renormalization $z \to z - 1$. Finally we mention that inclusion of H_2 in the above calculation would have destroyed the ladder structure because then the hole is already mobile at the Hartree-Fock level. Strictly speaking, this term is of course present (and of order t^2/U) in the Hubbard model (but not in the $t - J$ model).

4.2. The Coherent Spectrum: Trugman's Motion. — So far the hole is completely localized. In the absence of spin fluctuations it becomes mobile only when it manages to move without disturbing the antiferromagnetic background. As Trugman has observed [17], the simplest path to permit this is one where the hole hops around a plaquette one and a half times. The hole then moves to its nearest neighbor on the same sublattice while cleaning up the string of reversed spins in the end. In the diagrammatic scheme, we need to resort to vertex corrections to account for such paths. In fact, earlier studies have realized that Trugman's path corresponds to the leading nonzero vertex correction involving two loops [14, 18]. Within the present framework, the same process is described by a unique diagram as shown in Figure 6. The calculation for this bare 6th-order vertex correction is straightforward noting that both the hole lines and the particle-hole bubbles in the diagram are momentum independent and *retarded* in time. A slight complication occurs only due to the momentum dependence in the interaction vertex. For our purposes we only need to keep in mind that the vertex function at each interaction line in the diagram is determined by the momentum of the scattered hole in the intermediate state (the bold line in Fig. 4, as already encountered in obtaining Eq. (4.6)). The rules for calculating the diagrams are again the standard Feynman rules. The result for

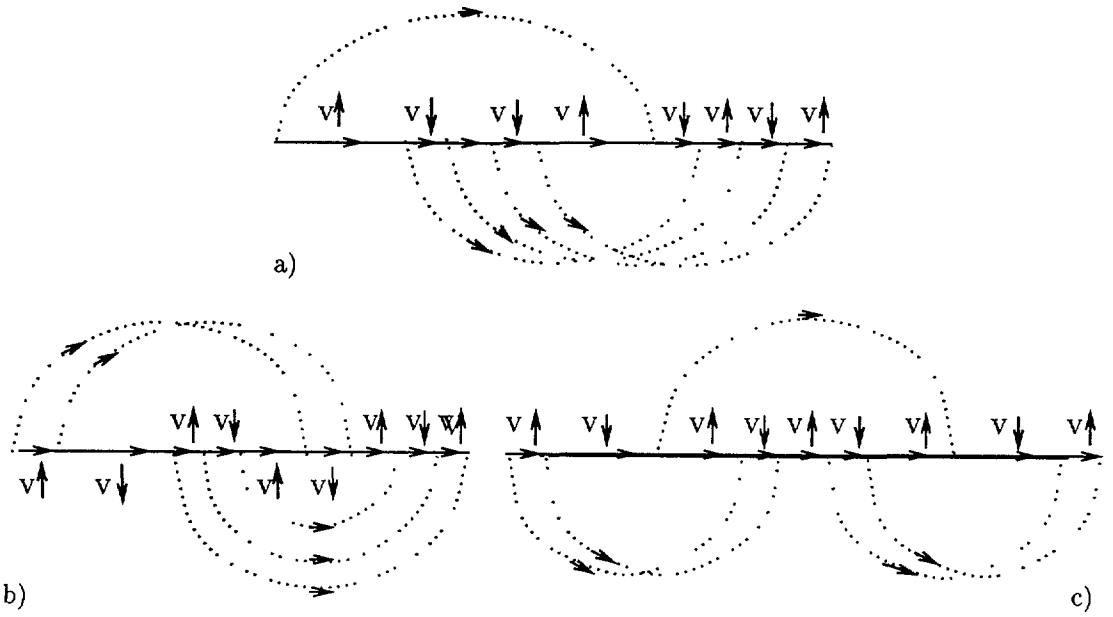

Fig. 7. — Nonzero vertex corrections at 10th order. The dotted line denotes a particle-hole bubble of opposite spins as in Figure 6. Note that the spin of the c-particle in each bubble is the same as that of the intermediate third hole.

the bare 6th order correction is then found to be

$$\Sigma_{\downarrow}^{v(6)}(\mathbf{k},\omega+i0^{+}) = \frac{z^4t^6}{(\omega-2J)^2(\omega-4J)^2(\omega-6J)}\frac{2}{N}\sum_{\mathbf{q}}\gamma_{\mathbf{q}}^2\gamma_{\mathbf{k}+\mathbf{q}}^2 \ . \tag{4.10}$$

The denominator in the above expression can easily be explained following Figure 6b. The hole loses an energy of $2J$ each time a particle–hole pair or a spin flip is excited, its energy reaches $\omega - 6J$ after three emissions and is only regained via three more steps in which it absorbs the emitted pairs (the spin flips are immobile once created). The maximal crossing of loops explains the order the hole must follow in the last three steps, the only possible path at 6th order is then the well-known Trugman loop (Fig. 6c). The delocalization of the hole is shown by the momentum dependence of the renormalized self-energy (4.10).

Obviously, with closed paths of longer lengths, the hole is able to move further away from its initial position. Evidently for any translation not affecting the spin structure it can only end up on the same sublattice, which in turn indicates that only vertex corrections of order $4n + 2$ will contribute. The next nonzero contribution then appears naturally at 10th order. Not surprisingly, the number of possible paths grows considerably as one goes to higher orders. Figure 7 describes the three processes responsible for the hole delocalization at 10th order. Apparently, the first two processes share a common feature in that in both cases the hole attempts to create a maximum number (here 5) of spin flips before it eliminates them again. They differ from one another only by the fact that they follow distinct paths in eliminating the spin flips. Figure 7a has maximal crossing of loops and is obviously the direct extension of the 6th order correction. Its real space configuration is therefore described by Figure 8a. The hole follows a fixed path (i.e., 1–2–3–4–5–6) and hops *two* loops minus *two* steps to its diagonal neighbor (i.e., its first neighbor on the same sublattice) while erasing the trace left behind. On

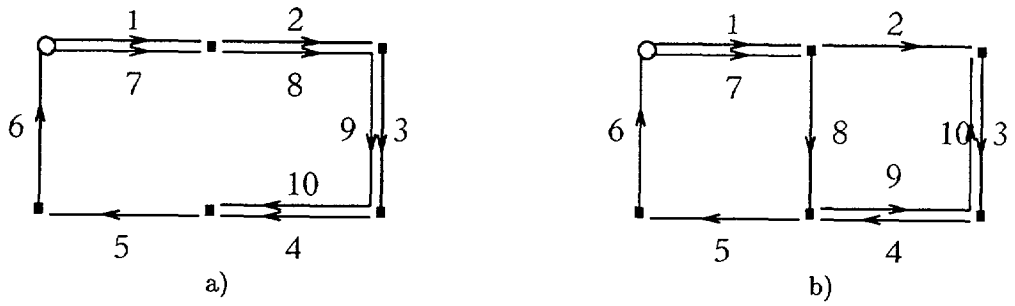

Fig. 8. — Schematical representation in real space of the graphs in Figure 7.

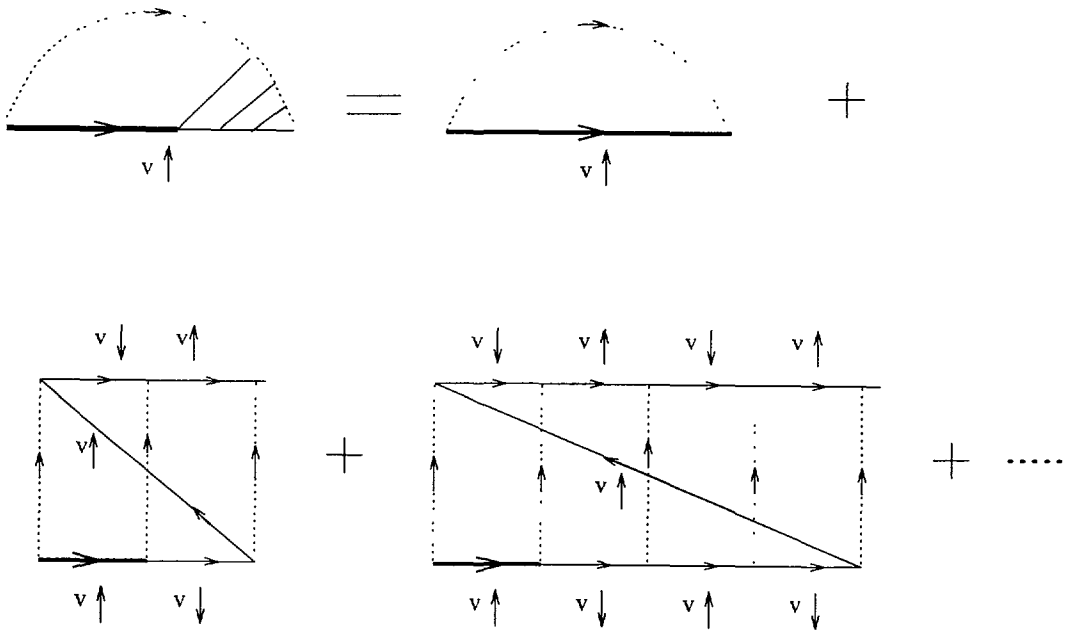

Fig. 9. — Maximally–crossed diagrams representing the coherent motion of a single hole in the Ising limit. Figures 6b and 7a are redrawn here in a different fashion to guide the eye.

the other hand, in Figure 7b the hole changes its path starting from the 8th step and ends up at one of its second nearest neighbors on the same sublattice (see Fig. 8b). Finally in the third process (Fig. 7c) we see at most three spin flips in the intermediate states and the hole runs along the path illustrated in Figure 7c and also moves to its second nearest neighbor sites.

To get an idea of how those higher order corrections affect the hole mobility, at present we will limit ourselves to the first category of closed paths. In other words, we shall only sum the series of maximally-crossed diagrams of $4n+2$ orders ($n = 1, 2, .$) as demonstrated in Figure 9 to get a picture of the mobile hole under Trugman's mechanism [19]. In a short while we shall actually show that as far as low energy physics is concerned, the dominant contribution comes only from the leading (6th) order vertex correction. Figure 9 is evaluated along the same lines that lead to equation (4.10) and we get:

$$\Sigma^{v}(\mathbf{k}, \omega + i0^{+}) = \frac{2}{N} \sum_{\mathbf{q}} \mathcal{G}(\mathbf{q}, \omega - 2J)\varepsilon_{\mathbf{q}}\{\varepsilon_{\mathbf{q}} + V(\mathbf{k}, \mathbf{q})\} \tag{4.11}$$

We have introduced selfconsistency in order to simultaneously account for the self-retracing paths discussed in the last section. Thus, in the absence of $V(\mathbf{k},\mathbf{q})$ this selfenergy just reproduces the incoherent result, equation (4.9). $V(\mathbf{k},\mathbf{q})$ sums the vertex corrections in Figure 9. Using the bare Green functions which are momentum-independent the momentum dependence of V is entirely due to the momentum dependence of the factors $\varepsilon_{\mathbf{k}}$ in equation (4.5). We then have

$$V(\mathbf{k},\mathbf{q}) = \frac{2}{N}\sum_{\mathbf{q}_2}\frac{\varepsilon_{\mathbf{q}_2}^2\varepsilon_{\mathbf{k}+\mathbf{q}_2-\mathbf{q}}(-t\varepsilon_{\mathbf{k}+\mathbf{q}_2})}{(\omega-2J)(\omega-4J)^2(\omega-6J)} + \frac{2}{N}\sum_{\mathbf{q}_2}\frac{\varepsilon_{\mathbf{q}_2}^2\varepsilon_{\mathbf{k}+\mathbf{q}_2-\mathbf{q}}(-t\varepsilon_{\mathbf{k}+\mathbf{q}_2})^3}{(\omega-2J)(\omega-4J)^2(\omega-6J)^2(\omega-8J)^2(\omega-10J)} + \ldots\} \ . \quad (4.12)$$

To help to understand this equation we note that $\mathbf{q}_2$ in the above expression is the hole momentum just one step before a complete closed path (see the diagonal hole line in Fig.9). In addition, the only momentum dependence comes from the interaction vertex, and summations over all but one internal momenta have been performed noting that $-t\varepsilon_{\mathbf{k}}$ is obtained by summing $\mathbf{q}$ in $\varepsilon_{\mathbf{q}}\varepsilon_{\mathbf{k}-\mathbf{q}}$. The omitted higher order terms in (4.12) can be obtained straightforwardly remembering that *bare* hole lines and bubbles are used inside the vertex part. The final result is determined by solving the following equation:

$$V(\mathbf{k},\mathbf{q}) = -\frac{2z^2t}{N}\sum_{\mathbf{k}'}\frac{\gamma_{\mathbf{k}'-\mathbf{k}}^2\gamma_{\mathbf{k}'-\mathbf{q}}}{\gamma_{\mathbf{k}'}}F(\mathbf{k}',\omega) \ , \quad (4.13)$$

$$F(\mathbf{k},\omega) = \frac{(zt^2\gamma_{\mathbf{k}})^2}{(\omega-2J)(\omega-4J)^2(\omega-6J)}(F(\mathbf{k},\omega-4J)+1) \ . \quad (4.14)$$

Without going into the details of a numerical solution, we can immediately learn two points by examining the above equation. First, as long as $J/t \ll 1$ close to the bottom of the Brinkman-Rice spectrum ($\omega \sim \omega_0 = -2\sqrt{z}t$) we have $F(\mathbf{k},\omega) \approx (zt^2\gamma_{\mathbf{k}})^2/\omega^4$. In other words, the higher order vertex corrections are quantitatively insignificant around the minimum of the spectrum since every additional two loops add a factor of roughly 1/16. Therefore, the mobility of the hole is dominantly determined by the leading vertex correction. The second point needs some elaboration. The statement is that in any event, the vertex correction above alone is not expected to give quantitative satisfaction. Since the point has in fact already shown up in equation (4.10), we take the case of the leading vertex correction to demonstrate the essential fact. Recall that in obtaining the preceding equations it is always implicitly assumed (by using Eq. (3.9)) that the energy cost to create a spin flip is $2J$. This is not correct in the presence of a hole. From Figure 6c we see that in fact it costs the hole only $3J/2$ to perform the first step, J for the next, and $J/2$ for the third step, and vice versa for the energy-recovering steps. The evolution of the energy cost for a hole moving around the plaquette is shown in Figure 10a. In the same manner, the J factors in both equation (4.12) and equation (4.14) are seen not to give a correct description of the energy cost in the intermediate states. As can readily be understood this failure is directly related to the Hartree–Fock approximation we have applied in the longitudinal channel (the third term in H_1): the intraband correlations between holes at different intermediate states have so far been neglected. The renormalizations due to the correlation effects in this channel can be easily taken into account at fixed order in the vertex corrections, as done in equation (4.15) below. However, a systematic procedure to all orders seems to be difficult to find because the energy cost in the intermediate states of a closed path is configuration-dependent. Take the 10th order maximally crossed diagram as example: we

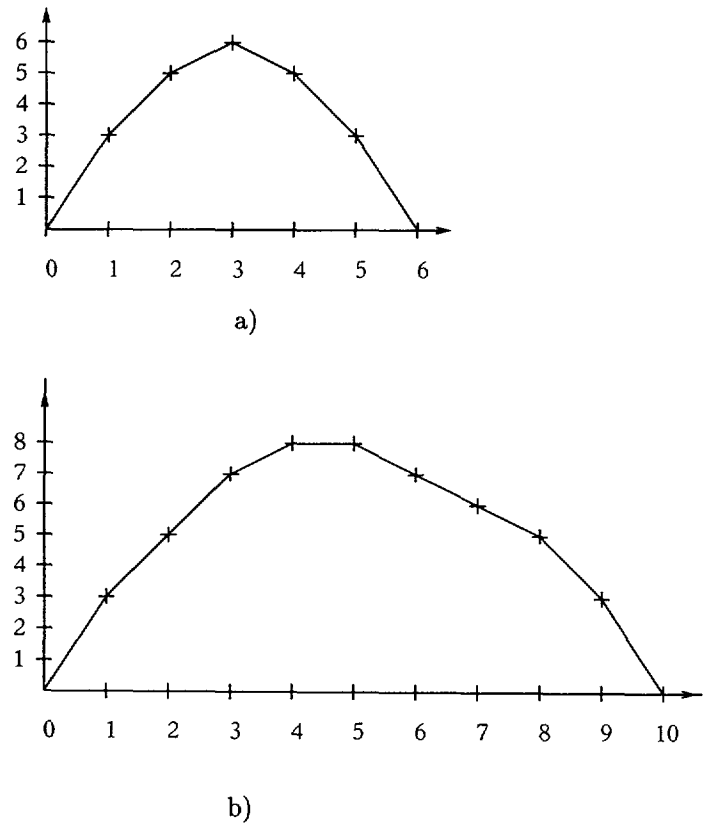

Fig. 10. — The evolution of the energy in the intermediate states immediately after the nth hopping step: a) for the leading vertex correction; b) for the 10th order maximally crossing diagram (see Fig. 7a).

see the energy evolution shown in Figure 10b which is apparently unrelated to what we have observed in Figure 10a. This situation is in sharp contrast with the situation of the previous section and more generally with all self-retracing paths [15] where we know that except for the first step the energy cost to extend the path by one step is always J.

After these remarks we now concentrate on the leading order vertex correction. This can easily be done by truncating the iteration equation (4.14) by its first order approximation. In order to take into account the correlations in the longitudinal channel we also include renormalizations so that the J factors agree with the analysis of the last paragraph (Fig. 10a). Formally this can be achieved (at fixed order in H_I) by using the second *and* the third term in H_1 as the zeroth order Hamiltonian. The final equation we then have is

$$\Sigma^v(\mathbf{k},\omega+i0^+)=\frac{2z^2t^2}{N}\sum_{\mathbf{q}}\mathcal{G}(\mathbf{q},\omega-3J/2)\{\gamma_{\mathbf{q}}^2+\frac{2z^3t^4}{NR(\omega)}\sum_{\mathbf{q}_2}\gamma_{\mathbf{q}}\gamma_{\mathbf{q}_2}^2\gamma_{\mathbf{k}+\mathbf{q}_2-\mathbf{q}}\gamma_{\mathbf{k}+\mathbf{q}_2}\}\ , \quad (4.15)$$

where $R(\omega)=(\omega-J/2)(\omega-3J/2)(\omega-5J/2)(\omega-3J)$. To recover what we should have obtained in the absence of renormalizations, we need only to replace $R(\omega)$ by $(\omega-2J)(\omega-4J)^2(\omega-6J)$ and $(\omega-3J/2)$ in the argument of $\mathcal{G}$ by $(\omega-2J)$.

We shall now solve the above equation numerically. Figure 11 shows our numerical results

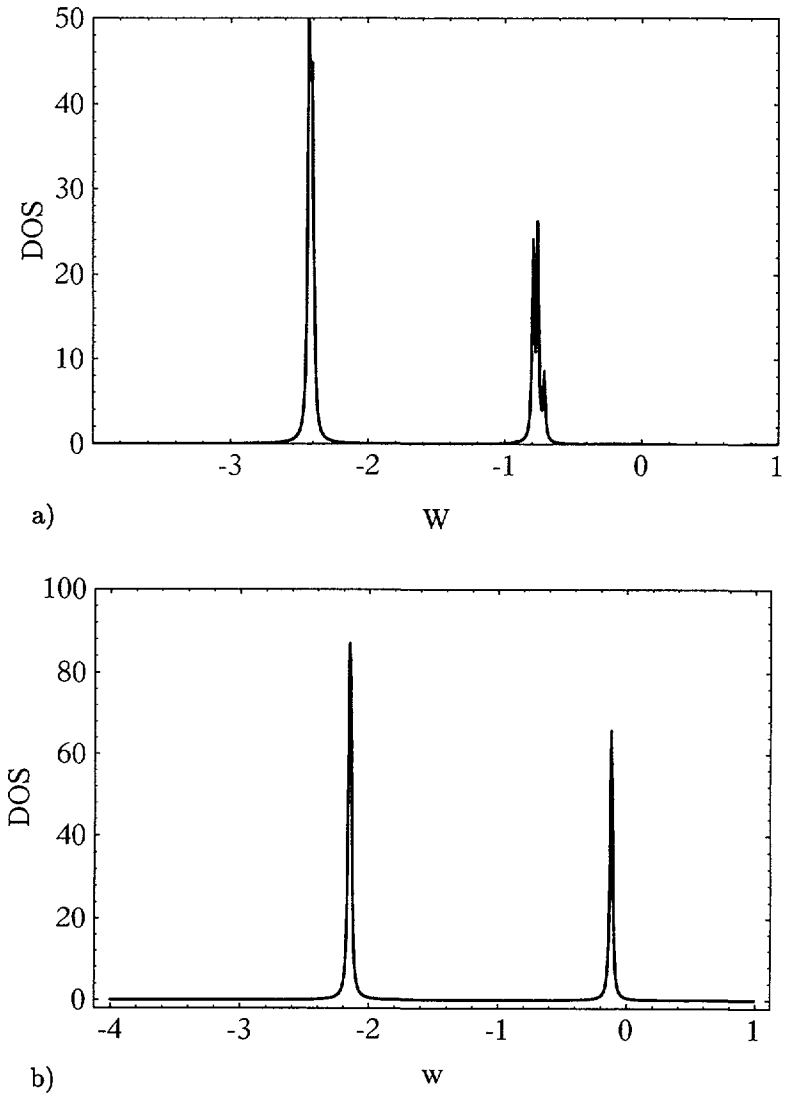

Fig. 11. — The density of states for a single hole in the Ising limit at $J/t = 0.5$, calculated on the 20-site cluster. A Lorentzian broadening with broadening parameter $\delta = 0.01$ is used: a) with renormalizations as explained in the text; b) without renormalizations.

for the density of states for $J = 0.5t$ on a cluster of 20 sites. Since our calculation is reliable only near the bottom of the spectrum and for relatively small J/t, one should note that the data on the high energy side of the spectrum does not make sense and is therefore omitted. In the following the discussion will be focused only on the lowest two peaks in the figure. First of all our numerical solution shows that the hole spectrum becomes dispersive with the introduction of vertex corrections and the ground state is located at $\mathbf{k} = (0, 0)$. The density of states around the lowest peak therefore broadens in contrast to the δ–peak in the Shraiman–Siggia limit. Secondly, the peaks shift to lower energies when including the renormalization,

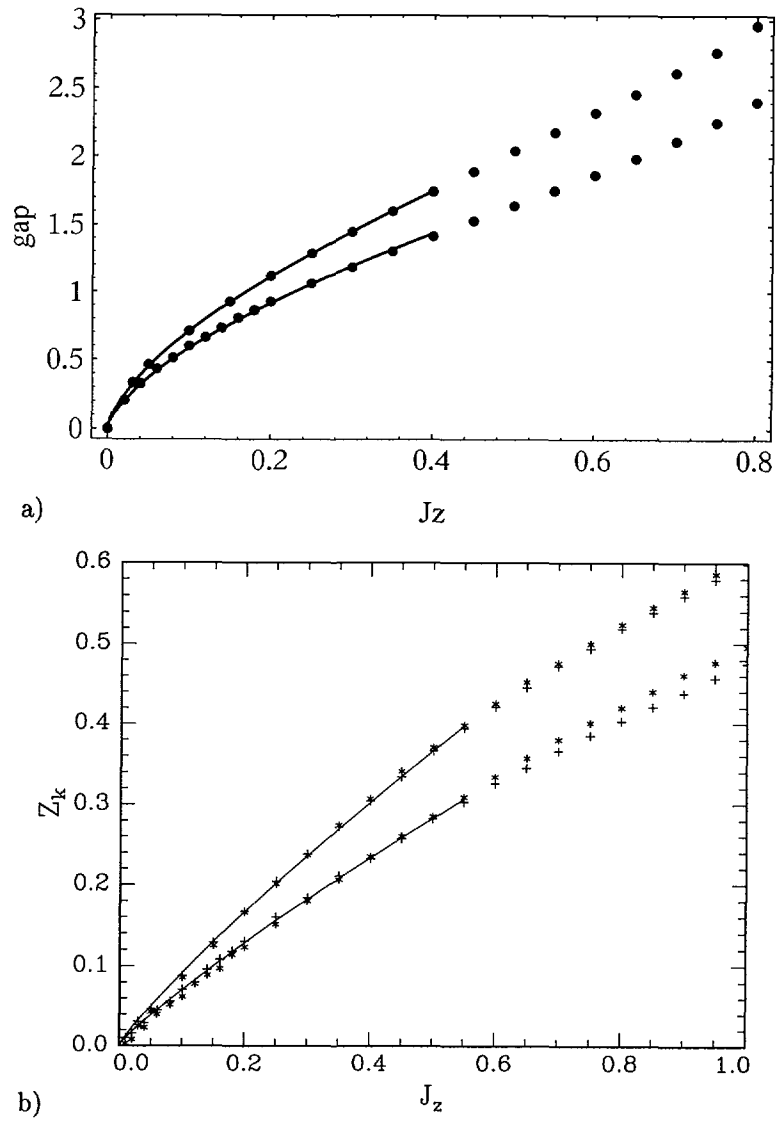

Fig. 12. — a) The gap Δ between the lowest two states as a function of J_z (Ising limit), with renormalization (lower curve) and without renormalization (upper curve) due to interactions in the longitudinal channel. The lines are fits to $\Delta = 2.610 J_z^{0.65}$ and $\Delta = 3.173 J_z^{0.65}$, respectively; b) the quasiparticle residue for $\mathbf{k} = (0,0)$, denoted by (+) and $\mathbf{k} = (0,\pi)$, denoted by (*), with renormalization (lower curves) and without renormalization (upper curves). The lines are fits to $Z_{\mathbf{k}=0} = 0.511 J_z^{0.86}$ and $Z_{\mathbf{k}=0} = 0.662 J_z^{0.86}$, respectively.

whereas the gap between the lowest two peaks becomes narrower as is shown in Figure 12a and can readily be explained from the form of $R(\omega)$. Also remarkable is the fact that the gap fits nicely a law $\sim a J_z^{0.65}$ for $J_z \leq 0.4$, with or without the renormalizations (see the figure caption for the prefactor a). This is close to the $J^{2/3}$–behavior in the Shraiman–Siggia limit. Let us now take a further look at the quasiparticle peak at the bottom of the spectrum. As

was explained before, the nature of the quasiparticle band does not depend too much upon the renormalizations we have included as long as J/t is small compared to unity. In Figure 12b we show quasiparticle residues for momenta at both the top and bottom of the band. With or without the renormalizations, the two residues are remarkably close to each other. The residue at the bottom of the quasiparticle band is always the smallest for $J_z > 0.3$. Moreover, $Z_{\mathbf{k}=0}$ shows a $J_z^{0.86}$–behavior for $J_z/t < 0.6$. These results agree well with numerical findings by exact diagonalization [20]. In fact, the structure of the quasiparticle band can actually be obtained analytically now that only the leading vertex correction are included. With the dominant pole approximation [16], we readily find that the quasiparticle band obeys:

$$\varepsilon_{\mathbf{k}} = \varepsilon_0 - \frac{J}{4z^2}\{(\cos k_x + \cos k_y)^2 + \cos(k_x + k_y) + \cos(k_x - k_y)\} \ , \tag{4.16}$$

where ε_0 is a constant. The quasiparticle is therefore seen to be confined within a narrow band of bandwidth J/z^2 and the minimum at $\mathbf{k} = (0,0)$. Finally, the ground state energy for the hole exhibits the $J_z^{2/3}$-behavior, simply following the string scenario. This should not be a surprise in view of the energy scale of the vertex correction near the bottom of the band.

4.3. The Coherent Spectrum: Spin Fluctuations. — Finally we switch back on the spin fluctuations which necessarily favor the delocalization of the hole. For simplicity, we shall take into account only the fluctuations in the transverse spin channel. The interaction part in H_1 is then composed of equation (4.5) and the the Heisenberg exchange in the transverse direction. As a immediate consequence we now have to consider also the process described by Figure 3b since the hole may easily face a "wrong-spin" neighbor created through spin fluctuations. It is certainly likely to hop to that neighbor in order to restore the local Néel ordering by absorbing the overturned spin. On the other hand, if the hole does hop to one of its Néel ordered neighbors, spin fluctuations will help to lower the energy by dispersing the newly created spin flip through the medium. In summary, spin fluctuations facilitate the propagation of the hole either by creating a trap in front of it or by immediately eliminating the trace it leaves behind. In this section we shall limit ourselves only to this new mechanism, while neglecting Trugman's mechanism assuming that the latter plays only a relatively minor role. This neglect is in fact justified by the numerically small prefactor in front of the **k**-dependent term in equation (4.16) ($J/4z^2 = J/64$).

In order to understand the diagrammatic description, let us look at the case in which a down spin hole initially sits on the origin and is surrounded by a local Néel environment. As it hops to one of its neighbors, it turns to an up spin hole at the new position and creates a spin flip at the origin. The flipped spin will now propagate in the medium because of spin fluctuations. Suppose that it approaches the hole again and ends up at one of its neighbors (on the even sublattice). For the reasons discussed above the hole would like to eliminate that overturned spin. This can happen in two different ways. It may either directly hop there, or it may hop one step more to another neighbor and let the newly created spin flip be eliminated together with the previous one through spin fluctuations. In the first case, all it involves in the intermediate states is the propagation of a spin flip from the origin to a site on the same even sublattice. The Feynman diagram for this process is therefore Figure 13a, where the propagation of the intermediate spin flip is given by $\chi_{11}(\mathbf{q},\omega)$ from equation (3.10). The self-energy of the hole is then determined by

$$\Sigma_{\downarrow}^{\mathrm{a}}(\mathbf{k},\omega + i0^+) = i\frac{2z^2t^2}{N}\sum_{\mathbf{q}}\int \frac{\mathrm{d}\omega_1}{2\pi}\mathcal{G}_{\uparrow}^{v}(\mathbf{k}-\mathbf{q},\omega-\omega_1+i0^+)\gamma_{\mathbf{k}-\mathbf{q}}^2\chi_{11}(\mathbf{q},\omega_1) \ . \tag{4.17}$$

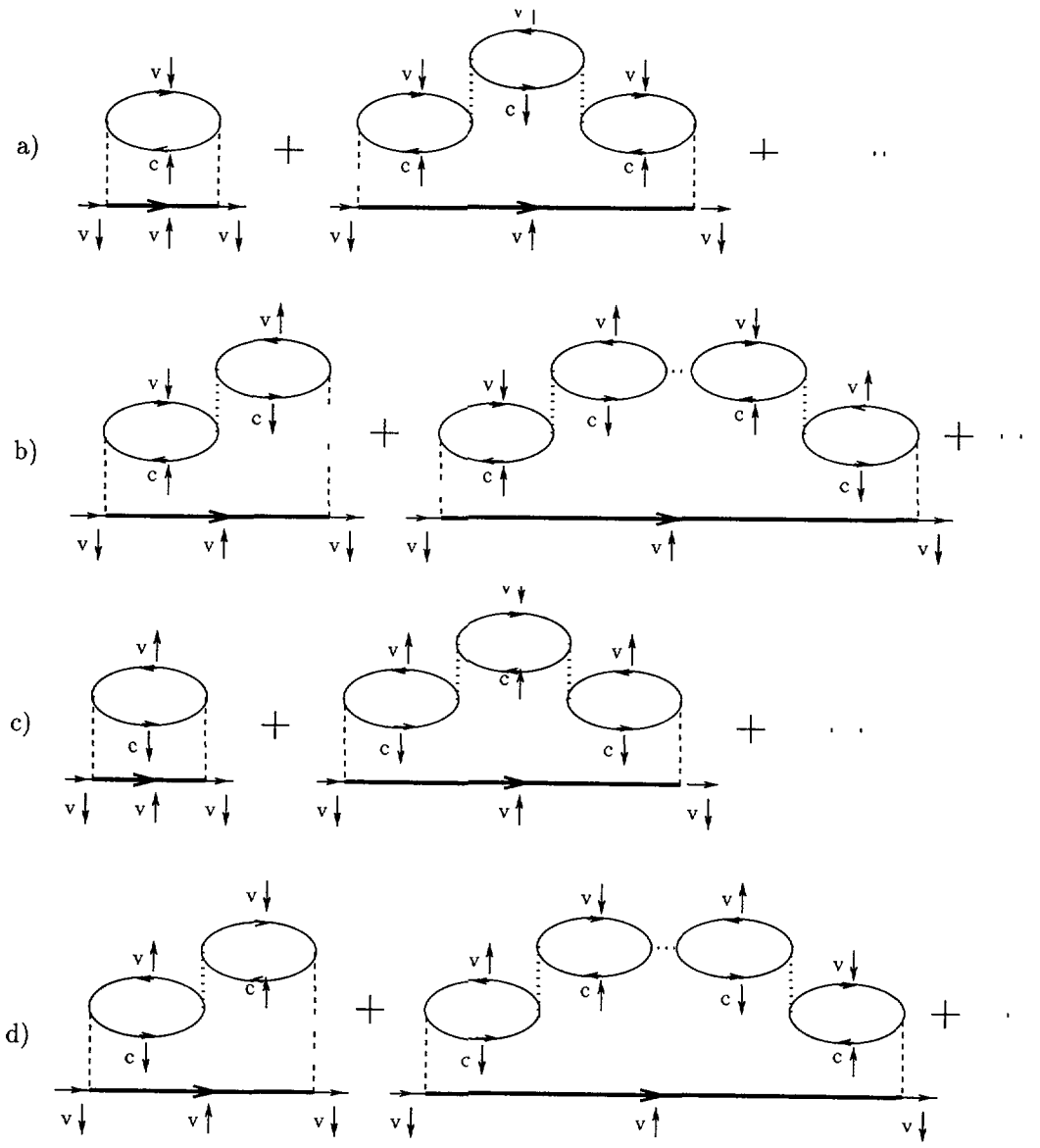

Fig. 13. — The self-energy diagram in the presence of spin fluctuations: a) the hole creates and then eliminates a spin flip at two successive hops; b) it creates a spin flip at each of the two hops; c) it first eliminates and then create a spin flip; d) it eliminates a spin flip at each of the two hops. In (a) and (b) the hole faces a Néel surrounding in the initial state, while in (c) and (d) it sees one of its neighbors disturbed in the initial state.

It differs from equation (4.8) only by the fact that the intermediate particle–hole pair is now able to propagate. On the other hand, in the second case we see an even number of particle-hole bubbles in the intermediate state between two successive hops of the hole. The process is

therefore described by Figure 13b and we obtain:

$$\Sigma^{b}_{\downarrow}(\mathbf{k},\omega+i0^{+}) = i\frac{2z^2t^2}{N}\sum_{\mathbf{q}}\int\frac{d\omega_1}{2\pi}\mathcal{G}^{v}_{\uparrow}(\mathbf{k}-\mathbf{q},\omega-\omega_1+i0^{+})\gamma_{\mathbf{k}-\mathbf{q}}\gamma_{\mathbf{k}}\chi_{21}(\mathbf{q},\omega_1) \quad . \tag{4.18}$$

Some attention should be paid to the interaction vertex (namely $\gamma_{\mathbf{k}}$) at the second hoping process. Its momentum dependence is determined by that of the hole in the final state (i.e., $\mathbf{k}$). As for the dynamical susceptibility, it is given by the off-diagonal term in equation (3.10) since we actually see the propagation of a pair of spin flips created by two successive hoppings. An analogous analysis applies if the hole is initially surrounded by distorted spins. The corresponding Feynman diagrams are shown in Figures 13c and 13d, from which we find:

$$\Sigma^{c}_{\downarrow}(\mathbf{k},\omega+i0^{+}) = i\frac{2z^2t^2}{N}\sum_{\mathbf{q}}\int\frac{d\omega_1}{2\pi}\mathcal{G}^{v}_{\uparrow}(\mathbf{k}-\mathbf{q},\omega-\omega_1+i0^{+})\gamma^2_{\mathbf{k}}\chi_{22}(\mathbf{q},\omega_1) \quad , \tag{4.19}$$

and

$$\Sigma^{d}_{\downarrow}(\mathbf{k},\omega+i0^{+}) = i\frac{2z^2t^2}{N}\sum_{\mathbf{q}}\int\frac{d\omega_1}{2\pi}\mathcal{G}^{v}_{\uparrow}(\mathbf{k}-\mathbf{q},\omega-\omega_1+i0^{+})\gamma_{\mathbf{k}}\gamma_{\mathbf{k}-\mathbf{q}}\chi_{12}(\mathbf{q},\omega_1) \quad , \tag{4.20}$$

respectively. Finally we integrate over frequency and sum equations (4.17)–(4.20) to get the total self-energy:

$$\Sigma_{\downarrow}(\mathbf{k},\omega) = \frac{2}{N}\sum_{\mathbf{q}} f(\mathbf{k},\mathbf{q})\mathcal{G}^{v}_{\uparrow}(\mathbf{k}-\mathbf{q},\omega-\omega_{\mathbf{q}}) \quad , \tag{4.21}$$

$$f(\mathbf{k},\mathbf{q}) = \frac{1}{2}z^2t^2\{(\frac{1}{\sqrt{1-\gamma^2_{\mathbf{q}}}}+1)\gamma^2_{\mathbf{k}-\mathbf{q}} + (\frac{1}{\sqrt{1-\gamma^2_{\mathbf{q}}}}-1)\gamma^2_{\mathbf{k}} - \frac{2\gamma_{\mathbf{k}-\mathbf{q}}\gamma_{\mathbf{k}}\gamma_{\mathbf{q}}}{\sqrt{1-\gamma^2_{\mathbf{q}}}}\} \quad . \tag{4.22}$$

The three terms appearing in the dressed vertex function $f(\mathbf{k},\mathbf{q})$ reflect the different scattering processes we have just discussed. (The factor 2 in the last term comes from the degeneracy in the processes leading to Σ^{b} and Σ^{d}). In particular $f(\mathbf{k},\mathbf{q})$ shows unambiguously that for a hole on the "nesting line" $|k_x|+|k_y|=\pi$ (where $\gamma_{\mathbf{k}}=0$), the only nonzero contribution comes from Σ^{a}. The hole having these particular momenta responds *only* to its Néel ordered neighbors. In addition, this hole only couples weakly to the dispersing low energy spin excitations, leading to $f(\mathbf{k},\mathbf{q}) \sim (\mathbf{q}_x+\mathbf{q}_y)^2/|\mathbf{q}|$, which in turn translates into $Im\Sigma \sim \omega^2$ in two dimensions [16]. In other words, quasiparticle behavior is well defined for these particular momenta. Secondly, quantum fluctuations play their full role in the hole dynamics only away from nesting wavevectors. Nonetheless, at these momenta none of the aforementioned scatterings by themselves support quasiparticle picture, as is clearly indicated by the individually divergent terms in (4.22). Only from the sum of all the terms do we obtain $f(\mathbf{k},\mathbf{q}) \sim |\mathbf{q}|$ or $Im\Sigma \sim \omega^2$ in the long wavelength limit and hence a quasiparticle behavior for the single hole. Finally, we notice that equations (4.21,4.22) are exactly the same as those obtained by Schmitt-Rink *et al.* [21] and by Kane *et al.* [16] using the slave-fermion technique. Numerical calculations based on equations (4.21) and (4.22) have been carried out by several groups [14, 22, 23] and they have indeed observed a well-behaved quasiparticle peak near the bottom of the spectrum. In particular, the ground state is found to be at $\mathbf{k}=(\pi/2,\pi/2)$ where, as we now see, a quasiparticle picture is well established. In reference [20] the numerical results obtained by the above groups were also compared with exact diagonalization results. Good agreement has been found concerning the $\mathbf{k}$ dependence of the quasiparticle residue, as well as its variation with J.

Before ending this section, we remind the reader that in studying the dynamics of a single hole we have assumed from the start the scattering processes involving energies of $O(U)$ are irrelevant as far as low energy properties of the single hole are concerned. To see exactly how this comes about we can in principle follow the same reasoning as for half filling. In the presence of spin fluctuations the selfconsistent RPA is then formed within the entire Hilbert space including scatterings involving double occupancies. The corresponding Feynman diagrams are those of Figure 13 except that the bare bubbles are replaced by those of Figure 1b. The final result is therefore again equation (4.21) and equation (4.22). In concluding this section, we also mention the recent calculation performed by Brenig and Kampf [24]. These authors have studied the dynamics of a single hole in the presence of a SDW antiferromagnet which is then extrapolated to the large-U limit. When a selfconsistent RPA scheme is adopted (as is done here), they have observed, along with the incoherent background, a quasiparticle band with a significantly reduced bandwidth. Moreover, the quasiparticle residue is found maximal at $\mathbf{k} = (\pi/2, \pi/2)$ and minimal at $\mathbf{k} = (0, 0)$. These observations agree with those derived from equations (4.21) and (4.22).

5. Summary

We summarize our main results in this section. We have shown that a transformation to a new basis facilitates the investigation of the crossover between weak and strong coupling limits of the Hubbard model. The new basis has been introduced via a Bogolyubov rotation. Its relation with the weak coupling method is seen from the fact that the transformation had previously been applied to the Hartree-Fock Hamiltonian which in turn served as the basis for further studies of fluctuation effects. Indeed, for the case of half filling, we have explicitly demonstrated in Section 3 the smooth crossover between two limits of Hubbard correlations. High energy scatterings have been shown to be irrelevant and are scaled away as U approaches the strong coupling regime. The correct spin wave mode we have derived in the final result is actually rather evident since the exact Heisenberg interaction in the transverse spin channel is contained in the low energy part of the effective Hamiltonian (i.e., Eq. (2.7)).

Within the new basis, we have further studied in detail the dynamics of a single hole in the antiferromagnetic background. Aside from the fact that we can diagrammatically distinguish the scatterings responsible for the low energy physics from those at high energy, we are also able to separate in Feynman diagrams the incoherent from coherent physical processes. In the Ising limit, we have analyzed a series of vertex corrections responsible for the hole delocalization and have concluded that the leading vertex correction dominates as far as low energy physics is concerned. In particular, for small J/t quantitative agreement is reached with exact calculations on small clusters regarding the low energy physics, namely the ground state and the nature of the coherent motion for a single hole near the bottom of the spectrum. The transverse spin fluctuations further support a quasiparticle picture in the case of a single hole. We have derived a selfconsistent equation which recovers previous results for the $t - J$ model which were obtained using slave-fermion methods. The numerical solution based on that selfconsistent equation also shows good agreement with exact solutions on small clusters. Finally, agreement is also found with results derived from direct extrapolation of weak coupling calculations recently done by Brenig and Kampf [24].

An important ingredient in the present calculation is the two sublattice antiferromagnetic spin structure. This is certainly correct in the case of one hole. However, finite hole–doping will certainly destroy the antiferromagnetic spin structure on which our discussions are based. The question concerning the stability of the quasiparticle picture and in particular its relevance to physical properties at finite hole densities therefore remains open. Further, the change of

physical properties as one goes from weak to strong correlation at finite doping has also not been fully clarified. We hope to address this question in a forthcoming investigation.

Appendix A

In this Appendix we explain the procedure which leads to equation (2.2), i.e., the Hubbard Hamiltonian written within the reduced Brillouin zone (RBZ).

By definition, the Fourier transform of a fermion operator at site j is expressed as

$$C_j = \frac{1}{\sqrt{N}} \sum_{\mathbf{k}}{}' e^{i\mathbf{k}\cdot\mathbf{j}} (C_{\mathbf{k}} + (-1)^j C_{\mathbf{k}+\mathbf{Q}}) \ , \tag{A.1}$$

where the summation over $\mathbf{k}$ covers the RBZ (i.e., $|k_x| + |k_y| \leq \pi$) and $\mathbf{Q} = (\pm\pi, \pm\pi)$. $C_{\mathbf{k}+\mathbf{Q}}$ complements $C_{\mathbf{k}}$ and together they run over every state in the whole Brillouin zone once and only once. Correspondingly, the number operator is written as

$$n_j = \frac{1}{N} \sum_{\mathbf{qk}}{}' e^{-i\mathbf{q}\cdot\mathbf{j}} (C^{\dagger}_{\mathbf{k}+\mathbf{q}} + (-1)^j C^{\dagger}_{\mathbf{k}+\mathbf{q}+\mathbf{Q}})(C_{\mathbf{k}} + (-1)^j C_{\mathbf{k}+\mathbf{Q}}) \ , \tag{A.2}$$

where again the summations for both $\mathbf{q}$ and $\mathbf{k}$ are confined to within the RBZ. In the meantime, $C_{\mathbf{k}+\mathbf{q}}$ and $C_{\mathbf{k}+\mathbf{q}+\mathbf{Q}}$ are complementary and cover the whole Brillouin zone centered at $\mathbf{q}$. The above expression can then be written compactly as

$$n_j = \frac{1}{N} \sum_{\mathbf{qk}}{}' e^{-i\mathbf{q}\cdot\mathbf{j}} \{\Psi^{\dagger}(\mathbf{k}+\mathbf{q})\Psi(\mathbf{k}) + (-1)^j \Psi^{\dagger}(\mathbf{k}+\mathbf{q})\sigma^1\Psi(\mathbf{k})\} \tag{A.3}$$

by defining a spinor $\Psi^{\dagger}_{\sigma}(\mathbf{k}) = (C^{\dagger}_{\mathbf{k}\sigma}, C^{\dagger}_{\mathbf{k}+\mathbf{Q}\sigma})$. The Hamiltonian can then readily be transformed noting that the following equality holds for the Fourier transform on sublattices:

$$\frac{2}{N} \sum_{r}{}' e^{-i\mathbf{q}\cdot\mathbf{r}} = \delta_{\mathbf{q},0} \ , \tag{A.4}$$

where the summation runs on either sublattice and $\mathbf{q}$ is defined within the RBZ. The U–term in the Hubbard model can then be expanded as

$$\begin{aligned} U \sum_{i} n_{i\uparrow} n_{i\downarrow} \quad = \quad & \frac{U}{N} \sum_{\mathbf{kk/q}} \{\Psi^{\dagger}_{\uparrow}(\mathbf{k}+\mathbf{q})\Psi_{\uparrow}(\mathbf{k})\Psi^{\dagger}_{\downarrow}(\mathbf{k}'-\mathbf{q})\Psi_{\downarrow}(\mathbf{k}') \\ & + \Psi^{\dagger}_{\uparrow}(\mathbf{k}+\mathbf{q})\sigma^1\Psi_{\uparrow}(\mathbf{k})\Psi^{\dagger}_{\downarrow}(\mathbf{k}'-\mathbf{q})\sigma^1\Psi_{\downarrow}(\mathbf{k}')\} \ . \end{aligned} \tag{A.5}$$

Equation (2.2) is thus derived.

Appendix B

In this Appendix we detail the procedure which transforms the susceptibility matrix, equation (3.1), so that it is represented by the r-operators, i e., in terms of Wannier functions. Following appendix A, the spin operator $S^{+}_{j} = C^{\dagger}_{j\uparrow} C_{j\downarrow}$ at site j can be written within the RBZ as

$$S^{+}_{j} = \frac{1}{N} \sum_{\mathbf{qk}}{}' e^{i\mathbf{q}\cdot\mathbf{j}} \{\Psi^{\dagger}_{\uparrow}(\mathbf{k}-\mathbf{q})\Psi_{\downarrow}(\mathbf{k}) + (-1)^j \Psi^{\dagger}_{\uparrow}(\mathbf{k}-\mathbf{q})\sigma^1\Psi_{\downarrow}(\mathbf{k})\} \ . \tag{B.1}$$

One can now Fourier transform the susceptibility matrix given in equation (3.1) within the RBZ and then write it in terms of r–operators by inverting equation (2.3). The final result for half filling is

$$\chi^{-+}(\mathbf{x},\mathbf{x}',t) = \frac{2}{N}\sum_{\mathbf{q}} \chi^{-+}(\mathbf{q},t)\mathrm{e}^{i\mathbf{q}\cdot(\mathbf{x}-\mathbf{x}')} \quad , \tag{B.2}$$

$$\chi^{-+}(\mathbf{q},t) = -\frac{i}{2N}\sum_{\mathbf{k}\mathbf{k}'} \left\{ f_1(\mathbf{k})f_1(\mathbf{k}') \begin{pmatrix} a_{11} & a_{12} \\ a_{21} & a_{22} \end{pmatrix} + f_1(\mathbf{k})f_2(\mathbf{k}') \begin{pmatrix} a_{12} & a_{11} \\ a_{22} & a_{21} \end{pmatrix} + f_2(\mathbf{k})f_1(\mathbf{k}') \begin{pmatrix} a_{21} & a_{22} \\ a_{11} & a_{12} \end{pmatrix} + f_2(\mathbf{k})f_2(\mathbf{k}') \begin{pmatrix} a_{22} & a_{21} \\ a_{12} & a_{11} \end{pmatrix} \right\} \tag{B.3}$$

where $f_1(\mathbf{k}) = (u_{\mathbf{k}} + v_{\mathbf{k}})(u_{\mathbf{k}-\mathbf{q}} + v_{\mathbf{k}-\mathbf{q}})$, $f_2(\mathbf{k}) = -(u_{\mathbf{k}} - v_{\mathbf{k}})(u_{\mathbf{k}-\mathbf{q}} - v_{\mathbf{k}-\mathbf{q}})$, and

$$\begin{pmatrix} a_{11} & a_{12} \\ a_{21} & a_{22} \end{pmatrix} = \langle T \begin{pmatrix} r^{v\dagger}_{\mathbf{k}\downarrow}(t) r^{c}_{\mathbf{k}-\mathbf{q}\uparrow}(t) r^{c\dagger}_{\mathbf{k}'-\mathbf{q}\uparrow}(0) r^{v}_{\mathbf{k}'\downarrow}(0) & r^{v\dagger}_{\mathbf{k}\downarrow}(t) r^{c}_{\mathbf{k}-\mathbf{q}\uparrow}(t) r^{v\dagger}_{\mathbf{k}'-\mathbf{q}\uparrow}(0) r^{c}_{\mathbf{k}'\downarrow}(0) \\ r^{c\dagger}_{\mathbf{k}\downarrow}(t) r^{v}_{\mathbf{k}-\mathbf{q}\uparrow}(t) r^{c\dagger}_{\mathbf{k}'-\mathbf{q}\uparrow}(0) r^{v}_{\mathbf{k}'\downarrow}(0) & r^{c\dagger}_{\mathbf{k}\downarrow}(t) r^{v}_{\mathbf{k}-\mathbf{q}\uparrow}(t) r^{v\dagger}_{\mathbf{k}'-\mathbf{q}\uparrow}(0) r^{c}_{\mathbf{k}'\downarrow}(0) \end{pmatrix} \rangle \tag{B.4}$$

As shown in equation (B.3), we need in general to calculate response functions with momentum dependent vertex functions $f_1(\mathbf{k})$ or $f_2(\mathbf{k})$ attached to either of the two external points. Nevertheless, for $U \gg t$, we can easily verify that χ^{-+} is dominated by the first term in equation (B.3). The remaining terms are smaller by at least a factor $O(J/U)$.

References

[1] Reger J. and Young A., *Phys. Rev. B* **37** (1988) 5978.

[2] Schrieffer J.R., Wen X.G. and Zhang S.C., *Phys. Rev. B* **39** (1989) 11663.

[3] Singh A. and Tesanovic Z., *Phys. Rev. B* **41**, 614 (1990).

[4] Schulz H.J., *Phys. Rev. Lett.* **64** (1990) 1445.

[5] Poilblanc D. and Rice T.M., *Phys. Rev. B* **39** (1989) 9749.

[6] Inui M. and Littlewood P.B., *Phys. Rev. B* **44** (1991) 4415.

[7] Shraiman B.I. and Siggia E.D., *Phys. Rev. Lett.* **62** (1989) 1564.

[8] Arrigoni E. and Strinati G.C., *Phys. Rev. B* **44** (1991) 7455.

[9] Auerbach A. and Larson B.E., *Phys. Rev. B* **43** (1991) 7800.

[10] Chubukov A.V. and Frenkel D.M., *Phys. Rev. B* **46** (1992) 11884.

[11] To compare with SWZ, we should note that $\chi^{+-}(\mathbf{q},\omega) = \chi^{-+}(\mathbf{q},-\omega)$. In addition, the following relations hold: $\chi_{SWZ}(\mathbf{q},\mathbf{q}) + \chi_{SWZ}(\mathbf{q}+\mathbf{Q},\mathbf{q}+\mathbf{Q}) = -(\chi^{+-}_{11} + \chi^{+-}_{22})$, $\chi_{SWZ}(\mathbf{q},\mathbf{q}) - \chi_{SWZ}(\mathbf{q}+\mathbf{Q},\mathbf{q}+\mathbf{Q}) = -(\chi^{+-}_{12}+\chi^{+-}_{21})$, $\chi_{SWZ}(\mathbf{q},\mathbf{q}+\mathbf{Q})+\chi_{SWZ}(\mathbf{q}+\mathbf{Q},\mathbf{q}) = -(\chi^{+-}_{11}-\chi^{+-}_{22})$, and $\chi_{SWZ}(\mathbf{q},\mathbf{q}+\mathbf{Q}) - \chi_{SWZ}(\mathbf{q}+\mathbf{Q},\mathbf{q}) = \chi^{+-}_{12} - \chi^{+-}_{21}$.

[12] More precisely, we have $\chi^{-+}(\mathbf{q},\omega) = -\chi^{-+}_{ST}(\mathbf{q},-\omega)$. The minus sign in front comes from the definition, while the minus sign before ω comes from the assumption we make in this paper that the spin points down on the even sublattice. The comparison with SWZ (Ref. [2]) can be done by using the relations given in reference [11].

[13] Shraiman B.I. and Siggia E.D., *Phys. Rev. Lett.* **60** (1988) 740.

[14] Martinez G. and Horsch P., *Phys. Rev. B* **44** (1991) 317.

[15] Brinkman W. and Rice T.M., *Phys. Rev. B* **2** (1970) 1324.

[16] Kane C.L., Lee P.A., and Read N., *Phys. Rev. B* **39** (1989) 6880.

[17] Trugman S.A., *Phys. Rev. B* **37** (1988) 1597.

[18] Johnson M.D., Gros C., and von Szczepanski K.J., *Phys. Rev. B* **43** (1991) 11207.

[19] For maximally-crossed diagrams of both 6th and 10th orders the final state of the hole hops is its diagonal nearest neighbor. This can not be generalized however. As can be best demonstrated at 14th order, higher order maximally-crossed diagrams also allow the hole to hop beyond its diagonal neighbors.

[20] Poilblanc D., Schulz H.J., and Ziman T., *Phys. Rev. B* **47** (1993) 3268.

[21] Schmitt-Rink S., Varma C.M. and Ruckenstein A.E., *Phys. Rev. Lett.* **60** (1988) 2793.

[22] Marsiglio F. *et al.*, *Phys. Rev. B* **43** (1991) 10882.

[23] Liu Z. and Manousakis E., *Phys. Rev. B* **44** (1991) 2414.

[24] Brenig W. and Kampf A.P., *Europhys. Lett.* **24** (1993) 679.